REPORT DOCUMENTATION PAGE

Form Approved
OMB No. 0704-0188

1. AGENCY USE ONLY	2. REPORT DATE	3. REPORT TYPE AND DATES COVERED
	AUG 97	Final 15MAR 94 - 14 MAR 97

4. TITLE AND SUBTITLE
NUMERICAL STUDIES OF THE PHYSICS AND OPERATION OF LTG MATERIALS AND DEVICES

5. FUNDING NUMBERS

61102F
2305/BS

6. AUTHOR(S)
Harold L. Grubin

7. PERFORMING ORGANIZATION NAME(S) AND ADDRESSES(S)

SCIENTIFIC RESEARCH ASSOCIATES, INC.
50 NYE RD., P.O. BOX 1058
GLASTONBURY, CT 06033

AFOSR-TR-97

0307

9. SPONSORING ORGANIZATION NAME(S) AND ADDRESSES(S)

AFOSR /NE
110 DUNCAN AVE., SUITE B115
BOLLING AFB, DC 20332-0001

... SPONSORING/MONITORING AGENCY REPORT NUMBER

F49620-94-C-0024

11. SUPPLEMENTARY NOTES

12a. DISTRIBUTION/AVAILABILITY STATEMENT

APPROVED FOR PUBLIC RELEASE: DISTRIBUTION UNLIMITED

12b. DISTRIBUTION CODE

13. ABSTRACT (*Maximum 200 words*)

This document summarizes Scientific Research Associates, Inc., (SRA) low temperature material studies, carried out under U.S. Air Force Office of Scientific Research (AFOSR) Contract F49620-94-C-0024. The study summarizes a model that was developed that is consistent with present low temperature growth (LTG) experimental studies. SRA's study included one-dimensional transient simulations and two-dimensional time independent constrained geometric studies. The broad aspects of the study indicate that annealed LTG GaAs is best represented as material containing precipitates with characteristics of embedded Schottky barriers. These embedded barriers are, in turn surrounded by defects. Carrier transport in annealed LTG GaAs is between the precipitates, with the details determined by the precipitate spacing, the concentration of traps, and properties of the surrounding traps. The two-dimensional studies provide numerical evidence that carriers travel between precipitates and are influenced, to first order, by the properties of the surrounding traps.

14. SUBJECT TERMS			15. NUMBER OF PAGES 32
Low temperature	Precipitates	Schottky barriers	16. PRICE CODE
Gallium Arsenide	Traps	Transport	

17. SECURITY CLASSIFICATION OF REPORT	18. SECURITY CLASSIFICATION OF THIS PAGE	19. SECURITY CLASSIFICATION OF ABSTRACT	20. LIMITATION OF ABSTRACT
UNCLASSIFIED	UNCLASSIFIED	UNCLASSIFIED	UL

Scientific Research Associates, Inc.

Final Report R97-9137F

Submitted to the Air Force Office of Scientific Research

August 1997

Numerical Studies of the Physics and Operation of LTG Materials and Devices

Table of Contents

Numerical Studies of the Physics and Operation of LTG Materials and Devices

Abstract

This document summarizes Scientific Research Associates, Inc., (SRA) low temperature material studies, carried out under U. S. Air Force Office of Scientific Research (AFOSR) Contract F49620-94-C-0024. The study summarizes a model that was developed that is consistent with present low temperature growth (LTG) experimental studies. SRA's study included one-dimensional transient simulations and two-dimensional time independent *constrained geometric* studies. The broad aspects of the study indicate that annealed LTG GaAs is best represented as material containing precipitates with characteristics of embedded Schottky barriers. These embedded barriers are, in turn surrounded by defects. Carrier transport in annealed LTG GaAs is between the precipitates, with the details determined by the precipitate spacing, the concentration of traps, and properties of the surrounding traps. The two dimensional studies provide numerical evidence that carriers travel between precipitates and are influenced, to first order, by the properties of the surrounding traps.

Numerical Studies of the Physics and Operation of LTG Materials and Devices

1. Introduction

This document summarizes Scientific Research Associates, Inc., (SRA) low temperature material studies, carried out under U. S. Air Force Office of Scientific Research (AFOSR) Contract F49620-94-C-0024.

Workers at SRA have been studying the electrical properties of annealed low temperature grown GaAs and have developed a model that is consistent with present experimental studies. The broad aspects of the study indicate that annealed LTG GaAs is best represented as material containing precipitates with characteristics of embedded Schottky barriers. These embedded barriers are, in turn surrounded by defects. Carrier transport in annealed LTG GaAs is between the precipitates, with the details determined by the precipitate spacing, the concentration of traps, and properties of the surrounding traps. SRA's study included one-dimensional transient simulations and two-dimensional time independent *constrained geometric* studies. Work covering the first two and one-half years of the study has been published in the *Journal of Applied Physics*. This study is incorporated as Appendix A to this final report.

Recent studies have focused on the details of the multidimensional transport. These studies, which are also summarized in this document, provide numerical evidence that carriers travel between precipitates and are influenced, to first order, by the properties of the surrounding traps. These studies have gone beyond the embryonic stage, but additional work is required to provide meaningful comparison to experiment.

2. Structure of the Report

The report is divided into five (5) sections including the appendix. Section 3 is a summary of the LTG studies including aspects of the preliminary two-dimensional studies. Section 4 discusses recommendations for additional new multi-dimensional LTG studies. Appendix A is a copy of the *Journal of Applied Physics* paper, summarizing the first two and one half years of the study.

3. Summary of LTG Studies

Most of SRA's LTG efforts involved a careful interpretation of experiment in light of the simulation studies of annealed LTG GaAs. Both transients and steady state studies were performed with emphasis on one-dimensional simulations. A wide variety of models were examined to explain the semi-insulating properties of GaAs LTG materials. These models included: (1) homogeneous defects; (2) clustered defects, (3) Schottky precipitates, (4) Schottky precipitates plus residual defects, (5) one-dimensional geometries, (6) cylindrical geometries, (7) spherical geometries, (8) transient photo-excitations, and (9) transport through multiple precipitates.

The broad conclusion of the study was that the precipitates in GaAs were three dimensionally confined metallic-like Schottky barriers, and that these precipitates were surrounded by defects. The Schottky barrier precipitates account for the dc semi-insulating properties of LTG GaAs; the transient properties require the incorporation of traps in the surrounding material. The reasoning that led to this conclusion is discussed in the **Journal of Applied Physics** paper contained in the appendix.

The major shortcoming of one-dimensional Schottky barrier precipitate calculations is that transport across the precipitate requires contributions from thermionic emission over the barrier or tunneling through the barrier. In actual devices carrier transport will likely involve percolation paths around and between precipitates. While a suitable treatment of percolating paths requires three-dimensional device simulations, much of the essential physics can be gleaned from scaled two-dimensional studies. Such two-dimensional studies were initiated under the current program and are summarized below.

3.1 Two Dimensional Calculations with Precipitates as Clusters of Defects

For the two-dimensional studies the precipitates were represented as cylinders. The height of each cylinder extended to $\pm\infty$, and so we are interested in transport-per-unit-device-depth. To set the stage for the study we first performed a number of base line, zero bias calculations. For example, figure 1 displays contours of constant density

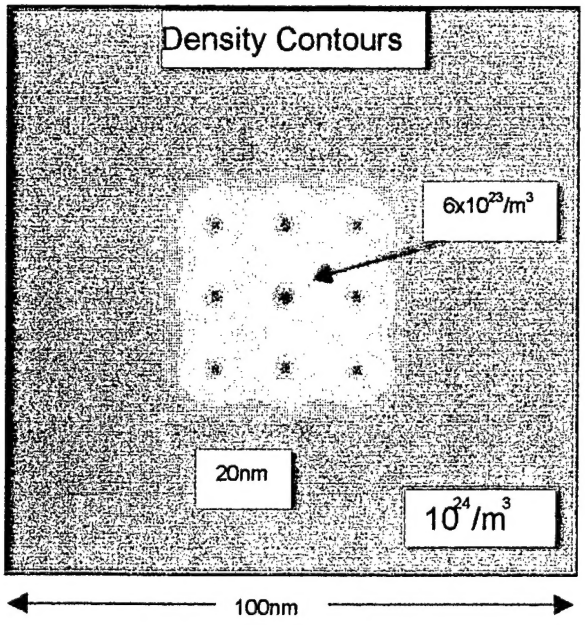

Figure 1. Density contours for a rectangular array of defect precipitates and a doping of $10^{24}/m^3$.

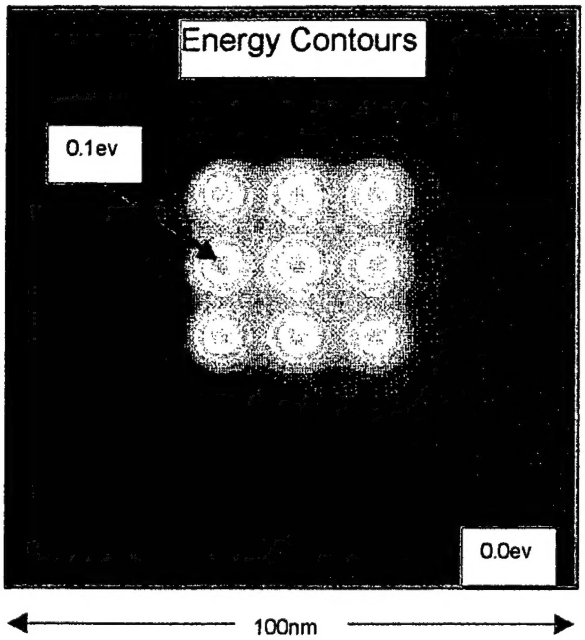

Figure 2. Constant conduction energy band contours for the array of figure 1.

for a rectangular array of nine precipitates, where the precipitates are represented as clusters of traps. The size of the structure is 100nm on edge, with 20nm separating the centers of the precipitates. The precipitates are surrounded by a trap free, uniform doping concentration of $10^{24}/m^3$. As indicated in figure 1, the concentration between precipitates peaks near $6x10^{23}/m^3$.

Figure 2 displays contours of constant conduction band energy corresponding to the charge distribution of figure 1. While there is apparent structure in the energy band profile, because of the negligible depletion surrounding the defect precipitates, the potential energy difference between the center of the precipitate and the surrounding substrate is a small 0.1eV. The situation for defect precipitates embedded within lower back-

ground concentration regions results in greater depletion as shown in figures 3 and 4. Here we display contours of constant conduction band energy for the same defect structure as that of figure 1 and 2---the difference is that the shallow donor density is reduced to $10^{22}/m^3$ in figure 3 and to $10^{23}/m^3$ in figure 4.

3.2 Two Dimensional Calculations with Precipitates as Schottky Barriers

Figures 5 and 6 are the Schottky barrier equivalents of figures 1 and 2. Here, we have a rectangular array of Schottky barrier precipitates each separated by 20nm. The barrier heights of the Schottky precipitates are each 0.8eV. The important physics differ-

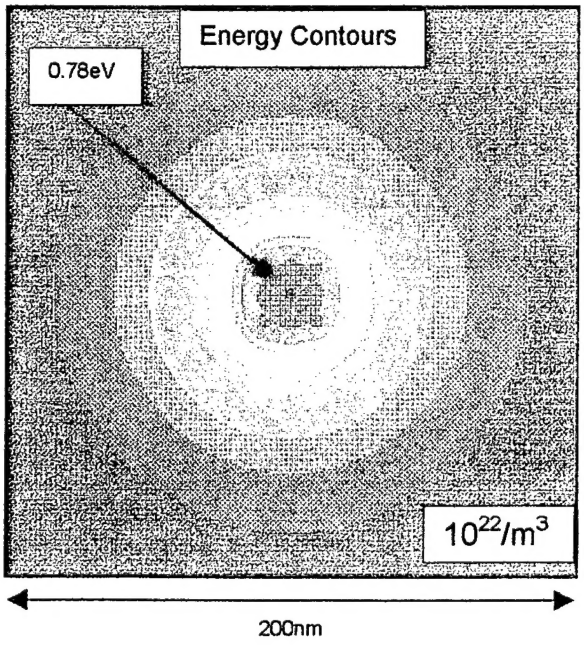

Figure 3. Contours of constant energy for a rectangular array of defect precipitates, surrounded by a doping of $10^{22}/m^3$.

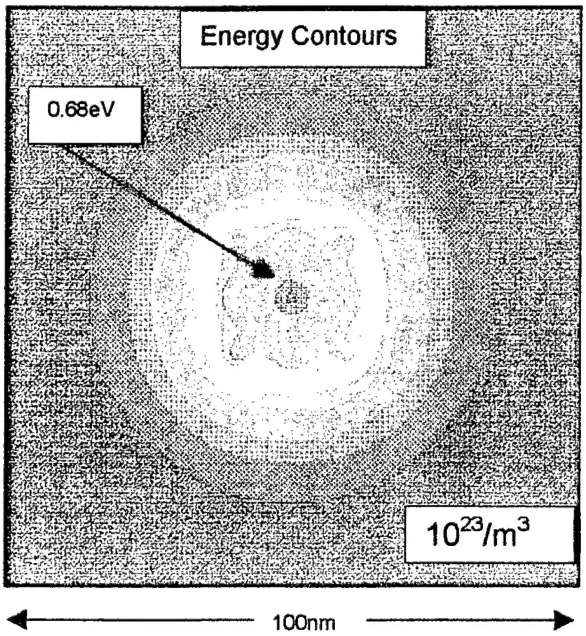

Figure 4. Contours of constant energy for a rectangular array of defect precipitates, surrounded by a doping of $10^{23}/m^3$.

ence between the results of the defect precipitates and the Schottky precipitates is that in the former the system is conductive, whereas for the Schottky precipitate the system is still non-conducting. (The origin of this difference is discussed in detail in the **Journal of Applied Physics Paper**, see appendix.) As seen in figure 5, the region approximately halfway between the precipitates sustains a density is approximately eight orders of

magnitude less than the shallow donor concentration. In the region surrounding the barrier the density is fourteen orders of magnitude smaller.

3.3 Current Flow in 2D Structures: Precipitates as Clusters of Defects and Why Space Charge Limited Current Appears in LTG Materials

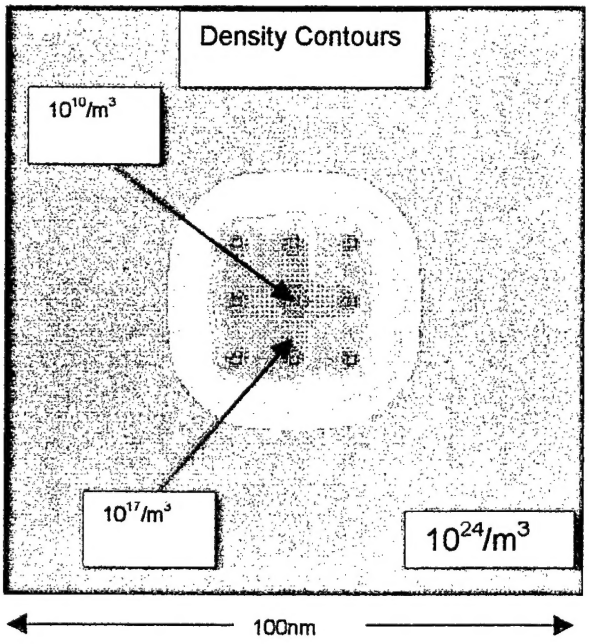

Figure 5. Contours of constant density for a rectangular array of Schottky precipitates, surrounded by a doping of $10^{24}/m^3$.

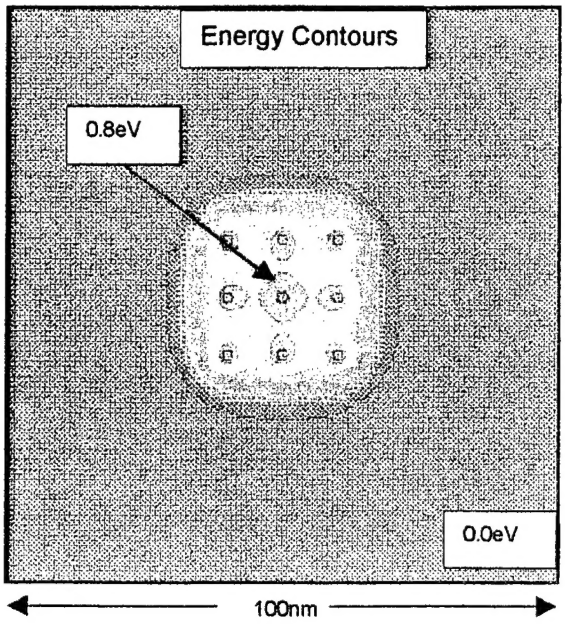

Figure 6. Contours of constant conduction energy band for the array of figure 5.

We were also able to perform calculations that illustrate the current paths in the presence of precipitates. These calculations are preliminary in that they were performed using the defect precipitate model, as the defect model is a *computationally more forgiving model.* (Similar calculations with Schottky barrier precipitates await future development.) These calculations, nevertheless, shed light on why the experimental characteristics show space charge limited properties. First, note that in the **Journal of Applied Physics** article, see appendix, we speculated that transport in the presence of precipitates would likely be between the precipitates where the carriers would be subject to the standard bulk transport properties-modified by the presence of overlapping depletion layers.

For these calculations, whose results are shown in figures 7-9, the potential energy is set to zero at the top of the structure and is equal to +0.5 eV at the bottom of the

structure. Figure 7 displays density contours under conditions of applied bias. (Figure 8 displays the density contours upon which we have superimposed the current streamlines.) First note the distortion of the depletion layers under bias. There is enhanced depletion surrounding the layer closest to the top of the structure. It is in this region where a larger fraction of the potential falls, as seen in figure 9. Thus there would appear to be a blocking region on the top part of the precipitate structure.

The juxtaposition of current streamlines and density contours in figure 8 shows current flowing from bottom to top. While we had difficulty in suitably registering the current streamlines with respect to the density contours the essential features of transport are clear from this picture. *Current flow is around the precipitates.*

Thus the broad picture of transport in annealed material dominated by metallic precipitates is a follows:

(1) Current paths are between precipitates.

(2) Carriers traveling between precipitates will sample the material characteristics of the host material, and be responsive to defects, traps, doping variations, etc. Carriers traveling between precipitates are able to sustain bulk-like trap filled limited transport. Transients will be determined by the transport of carriers between the precipitates. (Recent work at UCSB (Ibbetson's thesis) suggests a richer trap description

(3) The semi-insulating properties of the material are dominated by overlapping depletion regions associated with the Schottky barrier-like metallic precipitates.

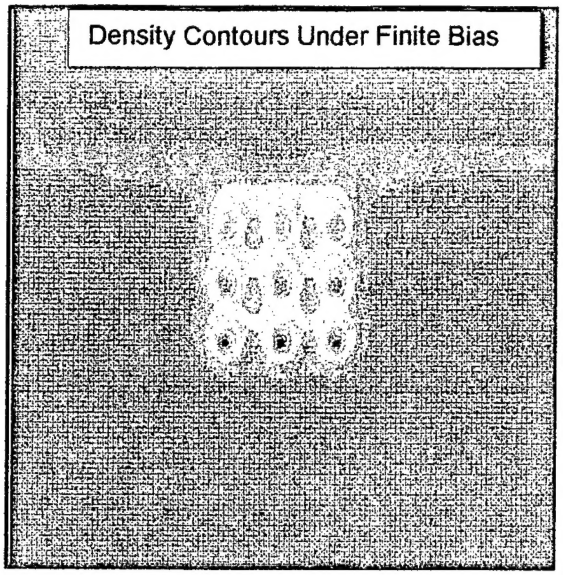

Figure 7. Constant density contours for the parameters of figure 2, under conditions of current flow at a bias of 0.5 volts.

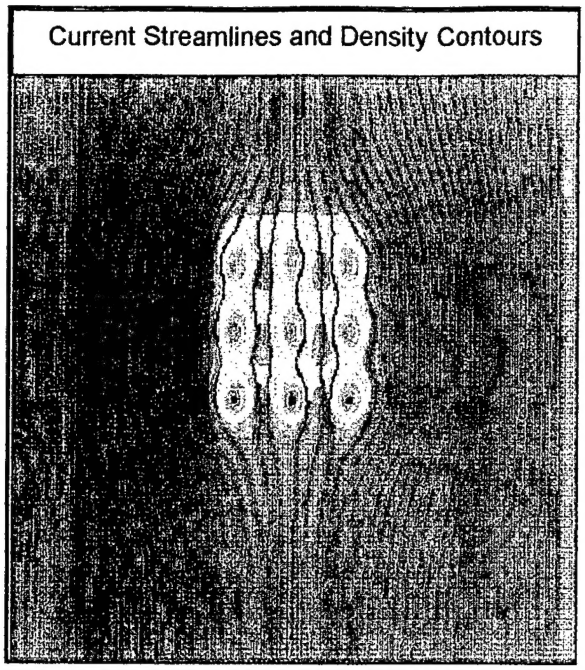

Figure 8. The constant density contours of figure 7, upon which current streamlines are superimposed.

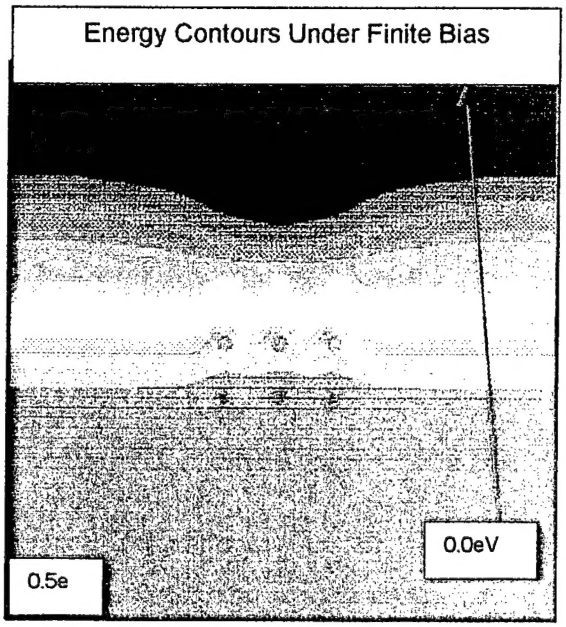

Figure 9. Contours of constant energy for the parameters of figure 7.

3.4 Dependence of 2D Results on Precipitate Configuration

We anticipate that the results of the above discussion do not depend, at least in a qualitative manner, on the configuration of the precipitates. To demonstrate this we began a study of the charge distribution associated with a hexagonal close packed array of precipitates. Figures 10 and 11 illustrate for precipitates represented as a cluster of de-

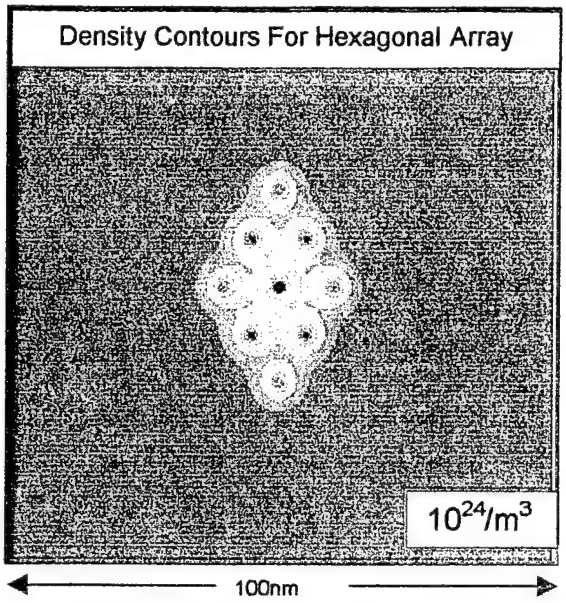

Figure 10. Contours of constant density for a hexagonal close packed array of defect precipitates for a doping of $10^{24}/m^3$.

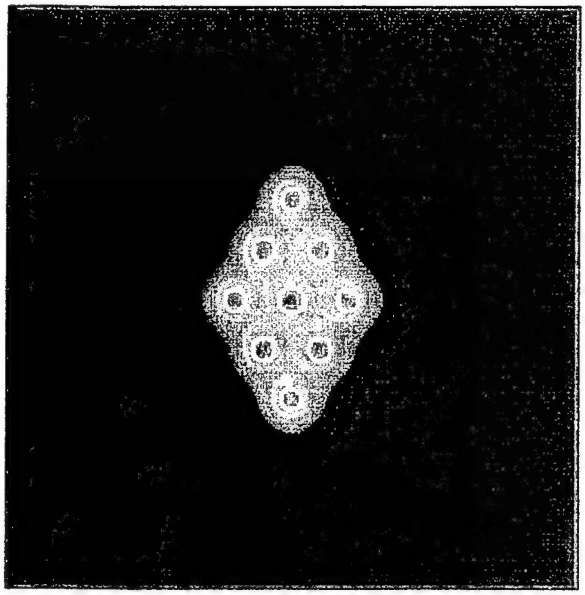

Figure 11. Contours of constant conduction band energy for the structure of figure 12.

fects. The precipitate is similar to that associated with figure2, the difference is the configuration. As can be seen the distribution of potential and density is qualitatively similar to that of the rectangular array. We have also taken the hexagonal close packed configuration and subjected the structure to an applied bias. As in the case of the rectangular array the current path is between the precipitates. Thus qualitatively similar behavior is seen under bias.

4. Recommendations

Our picture of transport in LTG material indicates that at a minimum a two dimensional picture is required. Here we have current flow between the precipitates, the magnitude of which is determined by the applied bias and the overlapping depletion re-

gions of nearest neighbor precipitates. As seen by the self-consistent calculations, represented by figures 7-9, the overlapping depletion zones are modulated by the applied bias. The picture is similar to a rectangular array of PBTs with floating gates, and indicates that the detailed properties of the material between the precipitates will have a first order influence on transport, and subsequent time dependent behavior. **This picture requires that we extend the two-dimensional modeling to include transient transport between metallic precipitates.**

Numerical studies of annealed non-stoichiometric low temperature grown GaAs

J. P. Kreskovsky and H. L. Grubin[a)]
Scientific Research Associates, Inc. Glastonbury, Connecticut 06033

(Received 23 August 1996; accepted 19 February 1997)

The means by which deep traps in annealed low temperature molecular beam epitaxy grown GaAs are responsible for its remarkable semi-insulating and short lifetime properties has been the subject of much discussion. For example, while low dc bias and high speed phototransient measurements can be explained as consequences of a homogeneous trap distribution in the non-stoichiometric material, experiments demonstrating the presence of electrically active precipitates must be dealt with. The study below, which is numerical, concludes that a consistent argument based on the presence of electrically active precipitates, coupled to a surrounding distribution of traps, will account for much of the observed experimental phenomena. © *1997 American Institute of Physics.* [S0021-8979(97)01711-8]

I. INTRODUCTION

Over the past several years considerable research has been performed in an effort to understand the favorable insulating and optical properties of GaAs grown by molecular beam epitaxy (MBE) at temperatures in the vicinity of 200 °C. Depending on the precise growth temperature and subsequent annealing, low temperature (LT) grown GaAs buffer layers have been found to reduce backgating, sidegating and light sensitivity in GaAs metal-semiconductor field-effect transistors (MESFETs).[1,2] Metal-semiconductor-metal (MSM) structures have also been fabricated using LT GaAs and tested as high speed photo conductive switches.[3,4]

The specific properties of LT GaAs have been associated with the presence of a very high density of defects, on the order of $10^{20}/cm^3$ in the as-grown material, and the subsequent precipitation of excess As after the material is annealed. Look *et al.*[5] concluded that prior to the annealing process the conductivity of the material is due to hopping conduction in a densely-populated "EL2"-like band. At anneal temperatures above 400 °C, the conduction mechanism becomes one of predominantly free-carrier conduction, with a corresponding reduction in the deep donor concentration. The resistivity of the material rises from values near 14 Ω cm for the unannealed material to values in excess of 10^6 Ω cm for annealed material. Additional early evidence of an EL2-like defect, related to the As_{Ga} defect, was reported.[6,7] More recent electro-optical measurements performed by Korona *et al.*[8] support this result. Early evidence of a deep acceptor with an ionization energy of $E_v+0.3$ eV was reported by Kaminska *et al.*.[9] This is also supported by positron annihilation evidence of deep acceptors, as reported by Haulojärvi *et al.*,[10] and by the results of Fang and Look[11] and McQuaid *et al.*.[12]

The highly resistive nature of LT GaAs has been attributed to the presence of defects in the as-grown material and the precipitation of arsenic in the annealed material. The fact that the material remains highly resistive, even when doped with shallow donors to levels approaching $10^{18}/cm^3$, lends support to the presence of traps at densities approaching $10^{18}/cm^3$ in the annealed material. The presence of defects can also explain the short carrier lifetimes satisfactorily. But the material and electrical characteristics of unannealed and annealed material are different, and Warren, *et al.*[13] postulated that As precipitates in the annealed material act, electrically, as buried Schottky barriers. In this model the depletion regions surrounding adjacent Schottky barriers overlap, thus creating a highly resistive material. The model of Warren *et al.*[13] has received considerable support from scanning tunneling microscopy (STM) studies of Feenstra *et al.*,[14] in which LT GaAs layers, grown at 225 °C, annealed at 600 °C and 800 °C, and *n*-type silicon-doped at $10^{19}/cm^3$, were studied. The presence of a significant density of midgap states induced by the precipitates demonstrated that the precipitates were capable of pinning the Fermi level, and the observation of local depletion surrounding the precipitates indicated that the precipitates were charged.

It has also been proposed[13,15] that the precipitates could act as recombination centers, thus accounting for the short carrier lifetimes. Look[16] indicates that for precipitate densities near $1\times10^{17}/cm^3$ the lifetime would be about 0.8 ps. This suggestion has been countered by the observation that the carrier lifetimes in the unannealed material, in which there are no precipitates, are of the same order in the annealed material. Whitaker[17] has reported lifetimes on the order of 180–260 fs for samples grown at 190 and 200 °C, with and without annealing at 600 °C (for 10–15 min). Because the lifetimes are inversely proportional to the defect densities, Whitaker's results[17] also suggest that annealing results primarily in the precipitation of the As^0_{Ga} defects which form the precipitates, while As^+_{Ga} and V_{Ga} defect densities should remain relatively unaltered.. However, other data suggests that As^+_{Ga} and V_{Ga} densities decline when the material is annealed.

One feature is clear from the above discussion: traps are responsible for the behavior of non-stochiometric GaAs. For annealed material there is the additional feature of precipitates. What are the properties of these precipitates? How may they be modeled? How do they affect transport? The pres-

a)Electronic mail: hal@srai.com

 0021-8979/97/81(11)/7326/19/$10.00

ence of precipitates suggests that current paths in LT GaAs will have percolation properties, and that simple bulk resistivity formulas may not provide an adequate explanation of device measurement. Indeed, the fact that several apparently different models for the material properties of LT GaAs can explain such features as the low field resistivity measurements and the carrier lifetime measurements, serves to highlight the limitation of explaining a rich set of material properties on the basis of current–voltage and photo-optical transient measurements. The results of Feenstra *et al.*[14] also force us to recognize the possibility that geometrical effects are important.

Numerical simulation is an ideal tool to examine these problems, with a full scale study requiring realistic device lengths, transients and three dimensions. Such studies await future efforts. For the present study, implementing numerical simulation procedures to study both LT GaAs material and device characteristics, *we have analyzed specific, but limited, device and material phenomena.* The simulation results follow a pattern leading to the conclusion that *spherical (three-dimensional confined) metallic-like precipitates, coupled to a surrounding distribution of traps, will account for much of the observed experimental phenomena.*

II. THE MODEL

The model is based upon the semiconductor drift and diffusion equations, including trap kinetics. The simulation is based upon the numerical solution of these equations. We have used the model to explore the electrical properties of devices with and without precipitates. The effects of precipitates were studied initially in a one-dimensional planar geometry, and then extended to single precipitates in spherical geometry. Specifically, we have:

(1) examined the kinetics of traps in materials with homogeneous and inhomogeneous trap distributions,

(2) modeled precipitates as a confined high density of traps; this model is referred to as the defect precipitate model (DPM),

(3) modeled precipitates as Schottky barriers; this model is referred to as the Schottky barrier precipitate model (SPM),

(4) examined an enhanced DPM which incorporates defects in the surrounding material, and

(5) examined an enhanced SPM, which also incorporates defects in the surrounding material.

Through the use of numerical simulation we were able to isolate the consequences of each model. A "roadmap" of the study, displayed as Table I, serves as a guide to the many different types of simulations performed. The "yes" and "no" comments identify the ability of the model to explain experimental observations.

III. THE EQUATIONS AND THE MODEL FORMULATION

The simulations of LT GaAs:As are based on the drift and diffusion equations, Poisson's equation, and rate equations for deep level donors and acceptors. The continuity equations, using the drift and diffusion relations for current densities, are:

TABLE I. Summary of results of the study. The "yes" and "no" comments identify the ability of the model to explain experimental observations.

Model studied	Precipitates	Resistivity	Phototransients
Uniform trap distribution	No	Yes	Yes
Defect precipitate model	Yes	Yes, marginal geometrical constraints	No
Schottky precipitate model	Yes	Yes	No
Enhanced DPM	Yes	Yes, marginal geometrical constraints	Yes
Enhanced SPM	Yes	Yes	Yes

$$\frac{\partial N}{\partial t} = +\frac{1}{e}\nabla\cdot\mathbf{J}_n + G_n - R_n, \tag{1}$$

$$\frac{\partial P}{\partial t} = -\frac{1}{e}\nabla\cdot\mathbf{J}_p + G_p - R_p \tag{2}$$

with the constitutive equations:

$$\mathbf{J}_n = -e(\mu_n N\nabla\phi_n - D_n\nabla N), \tag{3}$$

$$\mathbf{J}_p = +e(\mu_p P\nabla\phi_p + D_p\nabla P). \tag{4}$$

In equations (1) and (2), N and P are the electron and hole densities. In equations (3) and (4) μ_n and μ_p are, respectively, the electron and hole mobilities (with values given in Appendix B) and D_n and D_p, the respective diffusivities. G and R represent generation and recombination, which will be presented subsequently. For homogeneous material with variations in the doping concentration the potentials in equations (3) and (4) differ by the value of the band gap. For the embedded Schottky barrier model the precipitates are represented as material different from the host material (with a band structure consistent with the Anderson model) and the potentials, ϕ_n and ϕ_p, are given by:

$$\phi_n = \psi + \frac{\chi}{e} + \frac{k_B T}{e}\ell n N_c, \tag{5}$$

$$\phi_p = \psi + \frac{\chi}{e} + \frac{E_g}{e} - \frac{k_B T}{e}\ell n N_v. \tag{6}$$

Here χ is the electron affinity, E_g the bandgap, and N_c and N_v are the density of states for the conduction and valence bands. The quantity ψ is obtained from Poisson's equation:

$$\nabla\cdot(\epsilon\nabla\psi) = e[(N - N_0 - N_D^+) - (P + P_0 + N_A^-)], \tag{7}$$

where N_0 and P_0 are the densities of shallow dopants, and N_D^+ and N_A^- are ionized deep donors and acceptors. The total number of deep donor and deep acceptor traps are given by:

$$N_D^T = N_D^+ + N_D^0, \tag{8}$$

$$N_A^T = N_A^- + N_A^0. \tag{9}$$

In the following discussion we deal with both linear and spherical geometries. For spherical geometries, the divergence in equation (1) is: $(1/r^2)(\partial/\partial r)(r^2)$, and the left hand side of equation (7) becomes: $(1/r^2)(\partial/\partial r)(r^2\epsilon)(\partial/\partial r)$.

The kinetics of capture and emission from donors and acceptors determine the recombination rates for electrons and holes introduced into equations (1) and (2).

$$G_n - R_n = C_n(N_1^a N_A^- - N N_A^0) + C_n^+[N_1^d N_D^0 - N N_D^+] + G_n(external), \quad (10)$$

$$G_p - R_p = C_p^-(P_1^a N_A^0 - P N_A^-) + C_p(P_1^d N_D^+ - P N_D^0) + G_p(external), \quad (11)$$

where C_n and C_n^+ denote capture rate of electrons from acceptors and donors, respectively, and C_p^- and C_p denote capture rates of holes from acceptors and donors, respectively. The superscripts $+$, $-$, and on the donor and acceptor densities indicate an ionized or neutral state. We have also considered band-to-band recombination through $B(pn - n_i^2)$, with $B = 10^{-10}\text{cm}^3/\text{s}$. Band-to-band recombination effects are negligible, except for the very long time scales, and are ignored in most of the calculations.

The terms N_1 and P_1 are obtained from equilibrium conditions, and under non-degenerate conditions are approximated by the equations:

$$N_1^a = N_c \exp-[(E_c - E_a)/k_B T],$$

$$N_1^d = N_c \exp-[(E_c - E_d)/k_B T], \quad (12)$$

$$P_0^a = N_v \exp-[(E_a - E_v)/k_B T],$$

$$P_1^d = N_v \exp-[(E_d - E_v)/k_B T], \quad (13)$$

where E_c is the conduction band energy, E_v the valence band, E_d the energy level of deep donors, and E_a that of the deep acceptors.

The transients associated with the filling and emptying of the donor and acceptor states are governed by rate equations different from those of equations (1) and (2). For a single acceptor level and a single donor level these equations are:

$$\frac{\partial N_A^-}{\partial t} = C_p^-(P_1^a N_A^0 - P N_A^-) + C_n(N N_A^0 - N_1^a N_A^-), \quad (14)$$

$$\frac{\partial N_D^+}{\partial t} = C_n^+(N_1^d N_D^0 - N N_D^+) + C_p(P N_D^0 - P_1^d N_D^+). \quad (15)$$

The models studied using the above equations are:

A. The homogeneous model:

The material sustains a uniform distribution of deep level donors 0.69 eV below the conduction band and deep level acceptors 0.3 eV above the valence band. Concentration dependence was studied, as well as the effect of shallow dopants. Uniformly distributed donors and acceptors are most appropriate for unannealed material, but are included in this discussion of annealed material.

B. The defect-precipitate model (DPM):

This model assumes that the precipitate sites in annealed LT GaAs differ from the surrounding material only through an extraordinarily high local concentration of defects. Since the material constituting the precipitates is different from the host material, the conclusions of the study, with this assumption, are regarded as only qualitatively relevant. Assuming precipitates on the order of 60 A in diameter at a density of $10^{17}/\text{cm}^3$, and a total defect density of $10^{18}/\text{cm}^3$, the density of defects within a precipitate would be $8.85\times10^{19}/\text{cm}^3$ if all the defects were concentrated within the precipitates (see Appendix B). For the simulations we assume that these precipitates are periodically distributed throughout the material at a spacing of 200 A, which is consistent with a density of 10^{17} precipitates/cm^3. (The dependence of the results on precipitate density is also discussed.)

C. Computational Schottky barrier precipitate model:

Most device studies that incorporate Schottky barriers, e.g., field-effect transistor (FET) studies, do not deal with the specific properties of the Schottky barrier; rather, they treat the *effect* of the barrier as a boundary condition. However, this is not the case when the object of study is the Schottky barrier. For the present study, while we are not interested in the detailed properties of the Schottky barrier, treating the Warren *et al.*[13] Schottky barrier model as a boundary condition would not be fruitful. Instead, when simulating precipitates as buried Schottky barriers, the precipitate was represented as: (1) a zero band gap semiconductor with a specified offset voltage with respect to GaAs, in which (2) the electron and hole density are equal and high ($10^{20}/\text{cm}^3$) and where (3) everywhere within the material, except at the region surrounding the boundary of the zero band gap material and the GaAs material, there was local charge neutrality. In addition, by setting the hole mobility and diffusivity to zero within the precipitate, the holes become immobile and behave like ionized sites. The electron mobility and diffusivity are set to high values, which yields the desired low resistance. A generic representation of this model is illustrated in Figure 1, with the Schottky region to the left of the origin. While there are no traps within the modeled Schottky barrier region, the model permits a thin layer of deep level donors and acceptors at the semiconductor-Schottky interface to represent surface recombination effects. Because the model is new, a series of representative calculations are discussed in Appendix A.

D. Enhanced defect precipitate model:

This model starts with the defect precipitate model and adds traps in the region between the precipitates. These traps may have spatially varying properties.

E. Enhanced Schottky precipitate model:

This model starts with the Schottky precipitate model and adds traps in the region between the precipitates. These traps may have properties that vary spatially.

IV. SPATIALLY CONSTANT RESULTS: RESISTIVITY AND THE FERMI LEVEL IN THE ABSENCE OF PRECIPITATES

While annealed LTG GaAs contains precipitates and the measured resistivity is a property of percolating paths as well

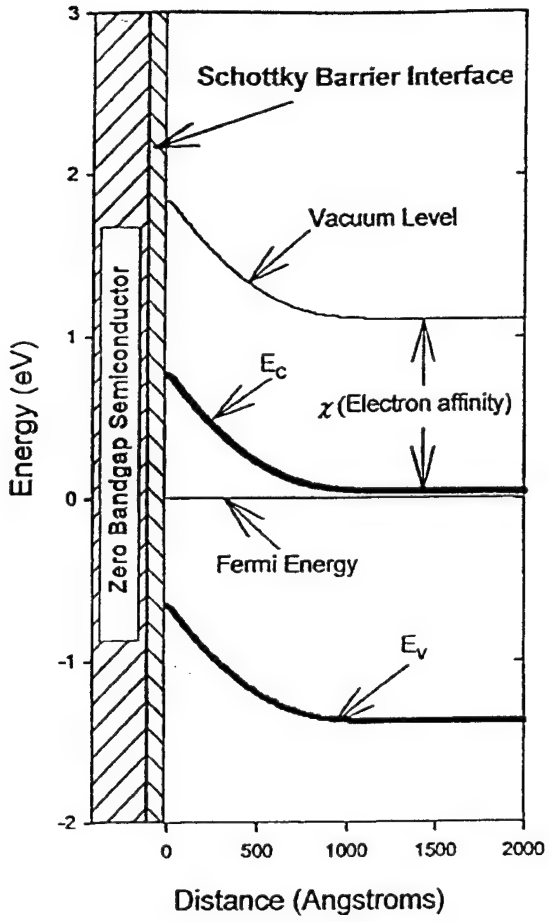

FIG. 1. Generic representation of a zero-band gap metal semiconductor configuration. The electron affinity varies discontinuously across the interface.

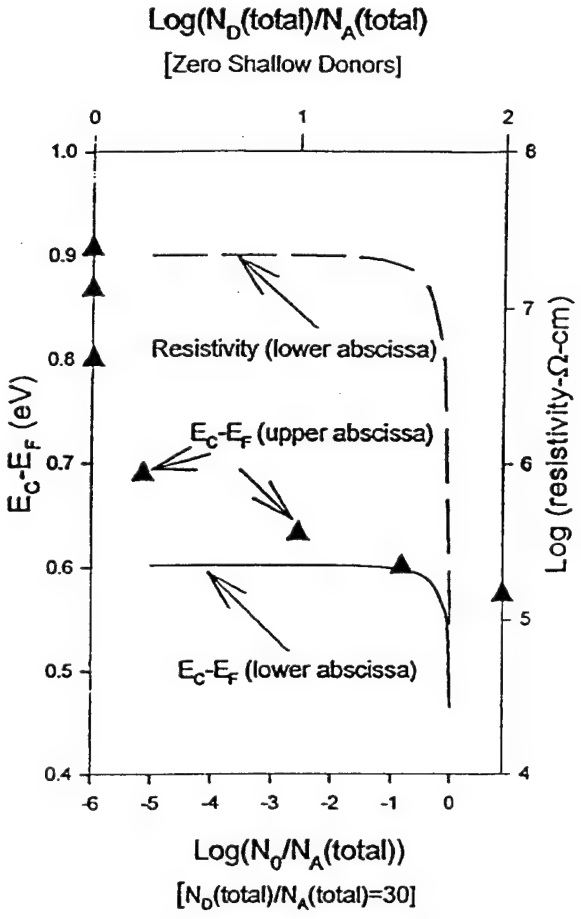

FIG. 2. For the case where $N_D^T/N_A^T=30$, the dependence on Fermi energy (solid line) and resistivity (dashed line) on the concentration of shallow donors (lower abscissa). For the case of zero shallow donors, the dependence of Fermi energy (solid triangles) as function of N_D^T/N_A^T (upper abscissa).

as the defect kinetics, the fact that simple models can account for some of the low field properties of non-stochiometric GaAs is addressed in this section. The resistivity of the material was computed for a uniform distribution of traps. Guided by various experimental investigations, we studied material with donors 0.69 eV below the conduction band and acceptors 0.3 eV above the valence band. The resistivity of the homogeneous material is $1/(Ne\mu_n+Pe\mu_p)$ where the densities are obtained from the kinetic equations subject to a condition of charge neutrality. The electron and hole densities in equilibrium are determined by the Fermi level, which in turn in this study is dominated by the position of the donor trap, the ratio of donor and acceptor traps, and, for shallow donors, the ratio of shallow donors to acceptor traps. This is displayed in Figure 2.

Figure 2 contains three plots. The solid line displays the relative position of the Fermi energy as a function of the ratio of shallow donors to total acceptors (lower abscissa) for the case where the ratio of deep donors to deep acceptors is $N_D^T/N_A^T=30$. This calculation was undertaken because of the experimental observation that annealed LT GaAs remains semi-insulating, even in the presence of a high concentration of shallow donors. The solid line results are approximately accounted for by the expression:

$$E_C-E_F=E_C-E_D+k_BT\ell n(1-N_0/N_A^T)-k_BT\ell n(N_D^T/N_A^T) \quad (16)$$

and show that for shallow donor densities less than $0.1N_A^T$ the conduction band remains very close to the undoped equilibrium position of 0.6028 eV above the Fermi level. To understand this result, we note that in the absence of shallow donors the deep acceptors are completely ionized, receiving an electron from the deep donors: $N_D^+=N_A^-$. As shallow donors are introduced (they are assumed to be completely ionized and degeneracy is not considered) the ionized deep donors are initially neutralized by an amount equal to the shallow doping density. For shallow donor densities below $0.1N_A^T$, the concentration of ionized deep donors is sufficient for the material to remain highly resistive; for shallow donor levels in excess of $0.1N_A^T$ the Fermi level moves up toward the conduction band.

The relative insensitivity of the Fermi energy to the concentration of shallow donors is reflected in values of the

resistivity, also shown in Figure 2 by a dashed line. For these calculations, where we assumed a mobility of 8000 $cm^2/V\,s$ for electrons and 400 $cm^2/V\,s$ for holes, the resistivity exceeds $10^7\ \Omega$ cm. The results shown in Figure 2 are typical of the results obtained for other ratios of donor to acceptor trap levels. The primary difference is the location of Fermi energy for low shallow donor doping.

For later discussion we include a plot of the Fermi level as a function of the ratio of donor traps to acceptor traps for the case of zero shallow donors. This is displayed by the closed triangles (upper abscissa) in Figure 2.

The above results show that a homogeneous distribution of traps could account for the dc semi-insulating properties of LT GaAs:As. From the experimental data (ignoring precipitates), after anneal the level of deep donor defects is on the order of $10^{18}/cm^3$, and from Figure 2 we can conclude that the material would retain the semi-insulating properties up to a shallow donor level approaching $10^{17}/cm^3$. For cases where the ratio of deep donors to acceptor is closer to 1.0, the shallow donor level will be even higher before the material becomes conducting.

V. DC CHARACTERISTICS FOR NIN STRUCTURES WITH A HOMOGENEOUS DISTRIBUTION OF TRAPS

The first level of complication is the *N*-doped–insulator–*N*-doped (NIN) structure with band conduction. We point out an even greater complication proposed by Luo *et al.*,[18,19] where conduction in annealed LT GaAs is a result of hopping between precipitates (we will discuss this later). Historically, one of the earliest numerical studies of band conducting semi-insulating properties of NIN GaAs was that of Horio *et al.*,[20] who concentrated on compensated material with an "*I*" region 20 μm long. A more recent study of relevance to the present article is that of Ibbetson *et al.*,[21] with a 2-μm-long annealed *I* LT-GaAs region. The Horio *et al.*[20] structure, which is significantly longer than that for which non-stochiometric GaAs is presently grown, is germane to the present discussion because it highlights the significance of trap-filled limited conduction as a possible transport mechanism.

For the structure of Horio *et al.*,[20] and for an *I layer* containing deep donors and *deep* acceptors at a ratio, $N_D^T/N_A^T=30$, as in Figure 2, we obtained current versus voltage (see Figure 3). (Calculations with parameters appropriate to Ibbetson *et al.*[21] are displayed in Figure 4.) Two sets of calculations were performed on the structure of Horio *et al.*,[20] identified by symbols: $N_D^T=6\times10^{14}/cm^3$ and $6\times10^{15}/cm^3$. No shallow acceptors are in the calculation. The contact regions are doped with shallow donors to a level of $2\times10^6/cm^3$. For comparison we repeated Horio *et al.*[20] (Figure 3, lines) for EL2 deep donor traps *and shallow acceptors*, at a fixed ratio of $N_D^T/P_0=11.11$; simulations were performed for $N_D^T=5\times10^{12}/cm^3$, $2\times10^{14}/cm^3$ and $5\times10^{15}/cm^3$.

While the details may differ, all five curves in Figure 3 display qualitatively similar behavior. In the low bias region, electrons injected into the *I* region are trapped and the resistivity of the structure is determined primarily by the resistivity of the *I* region. Until the trap-filled limit is approached, the resistivity remains relatively constant. As the trap-filled limit is approached, the traps can accept only a significantly reduced number of additional electrons, and a small increase in bias results in a flooding of the *I layer* with electrons and a corresponding dramatic drop in resistivity. Consequently, the current increases rapidly, with small bias increases. Beyond the trap-filled limit the velocity saturates and the current is governed by the space charge in the *I* region, which continues to increase with bias. The details follow.

For the curves labeled Horio *et al.*: at $N_D^T=5\times10^{12}/cm^3$, due to the low trap density, very few electrons need be injected into the *I region* before all the

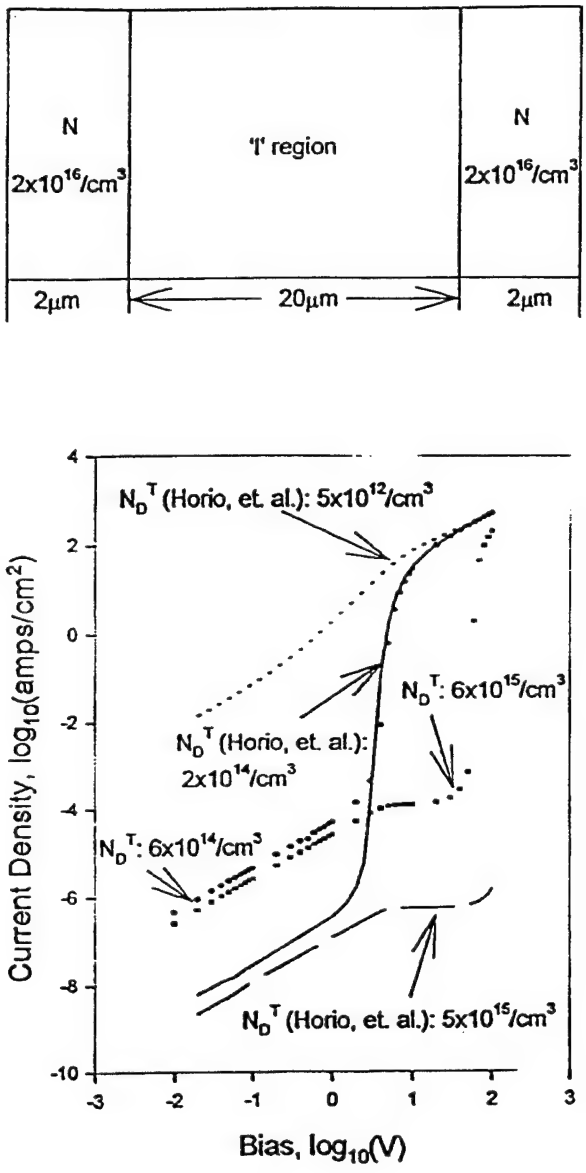

FIG. 3. (a) Structure for the NIN calculations. (b) Current–voltage relation with N_D^T as a parameter. Calculations identified by Horio *et al.* (see Ref. 20) are for a ratio of donor traps to shallow acceptors of 11.11. Calculations represented by symbols are for a ratio of donor traps to acceptor traps of 30. For all calculations the capture coefficients of Horio *et al.* (see Ref. 20), were used.

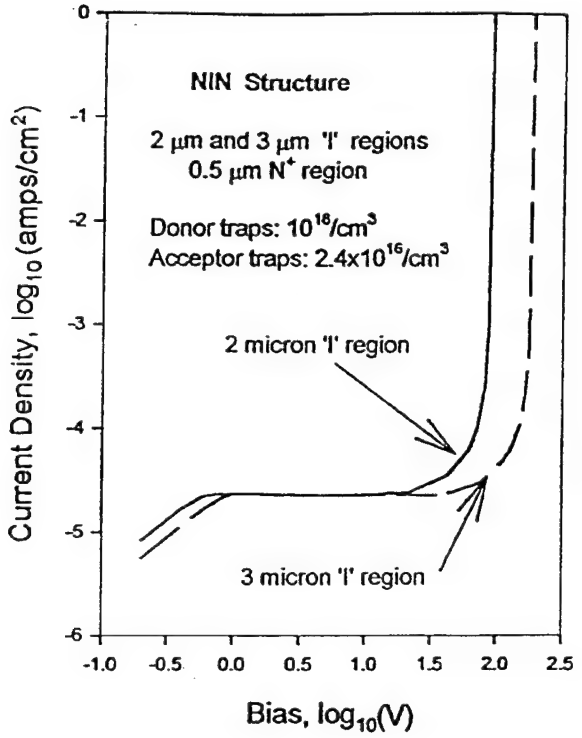

FIG. 4. Current–voltage characteristics for a 2 μm NIN structure with parameters similar to that of Ibbetson *et al.* (see Ref. 21). Results are also shown for an *I* region, 3 μm long.

traps are occupied; the resistivity is small. There is a soft transition between the ohmic and space charge limited regions. When the trap density is increased to $N_D^T=2\times10^{14}/\text{cm}^3$, there is substantially higher resistance in the low bias region, and the low bias and space charge limited regions are delineated by a sudden increase in current at the trap-filled limit. For a trap density of $N_D^T=5\times10^{15}/\text{cm}^3$ the resistance is further increased; because additional bias is needed to provide enough electrons to neutralize the traps, the presence of velocity saturation begins to affect the *IV* curve in the form of saturation below the trap-filled limit.

The $N_D^T/N_A^T=30$ calculations with acceptor traps (symbols in Figure 3) are qualitatively similar to those of Horio *et al.*[20] The resistivity increases as the concentration of donor traps increases. The effects of velocity saturation, prior to trap-filled limited transport at higher donor trap concentrations, delays the reduction in resistivity associated with trap-filled limited transport. Differences with Horio *et al.*,[20] e.g., comparing the latter resistance for $N_D^T=5\times10^{15}/\text{cm}^3$ to the deep acceptor trap calculations with $N_D^T=6\times10^{15}/\text{cm}^3$, are attributed to differences in the Fermi level.

The study of Ibbetson *et al.*[21] was an experimental and analytical investigation of space charge limited currents in nonstoichiometric GaAs. The *I* region was 2 μm thick and was separated from an N^+ buffer by a 20 A AlAs layer. The experimental results of Ibbetson *et al.*,[21] show *apparent* trap-filled limited operation. The qualifier arises because there was neither a discussion of breakdown, nor of the length dependence of the voltage at which the current shows the sharp increase. Luo *et al.*[19] argue that the threshold voltage for trap-filled transport varies as the square of the length of the *I* region, whereas breakdown varies linearly with length. Ibbetson *et al.*,[21] using a set of boundary conditions that were equivalent to pure drift current far from the junction, computed *I-V* curves that displayed saturation, but none of the trap-filled limit conductivity properties seen in Figure 3.

We performed an NIN calculation for the Ibbetson *et al.*[21] structure (see Figure 4). In our study the AlAs layer was ignored, the *I* region was 2 μm long, and the two end N^+ regions were each 0.5 μm long, with a density of $10^{18}/\text{cm}^3$. For this calculation the donor traps were situated at 0.73 eV below the conduction band, the mobility of the electrons was 1900 $\text{cm}^2/\text{V s}$, $N_D^T=10^{18}/\text{cm}^3$, $N_A^T=2.4\times10^{16}/\text{cm}^3$, which is an order of magnitude smaller than that used in the simulation study of Ibbetson *et al.*.[21] The acceptors were treated as traps with densities chosen to provide resistance values similar to experimental values. Additionally, velocity saturation in our calculation is 8×10^6 cm/s as opposed to 5×10^6 cm/s for Ibbetson *et al.*.[21] These parameters yield the results shown in Figure 4. (The calculations were repeated with shallow acceptors; there was no change in the results.)

The Figure 4 calculations display low bias resistivity results similar to those of Ibbetson *et al.*.[21] The calculations are classic trap-filled limit characteristics, with the high current levels at a voltage threshold somewhat higher than that of the experimental results. But the results of Figure 3 suggest that suitable tweaking of the input trap densities could yield matching voltage thresholds. The length dependence of the threshold for the onset of trap-filled current was also examined. The longer the *I* region, the higher the value of the threshold voltage for high current values. This is seen in the current–voltage curve for a structure with a 3 μm long *I* layer. For calculations with *I* layer lengths of 2, 3, and 4 μm, the length dependece of the voltage at which the current increased catastrophically is given approximately by $V_{\text{threshold}}\propto L^{1.8}$, which is somewhat less than the classic space charge limited behavior which varies as the square of the device length. The role of velocity saturation in the dependence of the threshold voltage must be assessed.

While the simple model without precipitates appears to account for the broad *IV* characteristics of NIN LT GaAs structures, it is premature to conclude that transport in LT GaAs is trap filled and then at higher bias levels space charge limited transport. Important unknowns here are the capture coefficients. The calculations of Figure 4 were performed using the capture coefficients of Horio *et al.*[20] (see Appendix B for values). We then repeated the calculations of *IV* with changes in the capture coefficients (0.1× standard, 10× standard, 100× standard), with the resulting simulations showing significant changes in the hole density. But the magnitudes of the hole density were small and did not change the input into Poisson's equation, nor did they contribute to the total current in any significant manner. As a result, the *IV characteristics were unchanged.* Additionally, for a given set of deep donor trap levels the results were insensitive to the properties of the acceptor traps. For the default set of capture coefficients, the *IV* was unchanged when the deep acceptor

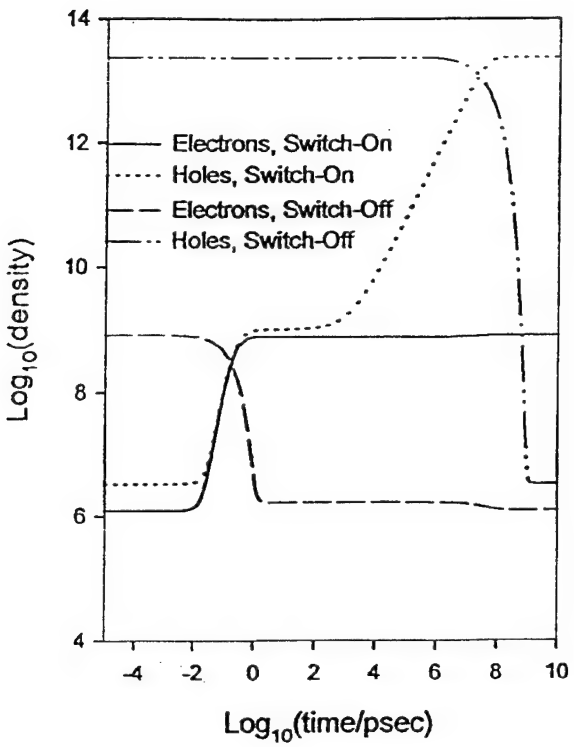

FIG. 5. Transient response of electrons and holes in the center of an NIN structure following the switch-on of 100 mW/cm^2 of band gap radiation, and the subsequent switch-off transient.

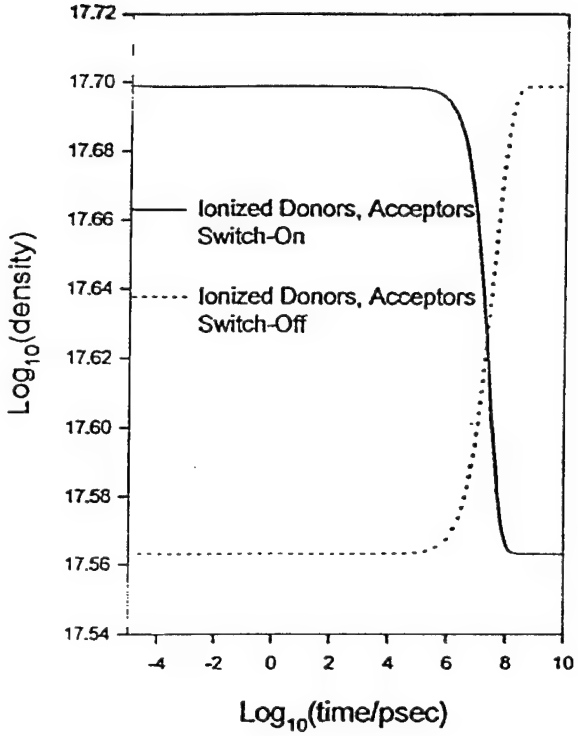

FIG. 6. As in Figure 5 but for the ionized donors and acceptors.

traps were replaced by shallow acceptor traps. This latter result is likely to be altered in the presence of shallow donors of any consequent density. *If there is anything that this preliminary model suggests, it is that dc measurements are not sensitive to some of the material properties of annealed nonstoichiometric GaAs. Transients should, of course, be sensitive to capture coefficients, and we deal with this next.*

VI. THE HOMOGENEOUS DEFECT MODEL; TRANSIENT RESPONSE FOLLOWING PHOTOGENERATION

As seen below, numerical simulation teaches that the transient response of LT GaAs to photoexcitation is sensitive to material properties We first illustrate this for the NIN structure with the dimensions of Figure 3, with the *I layer* modeled as LT GaAs with: (i) a homogeneous distribution of defects, (ii) capture coefficient values of Horio *et al.*,[20] (iii) $N_D^T/N_A^T=2$ and (iv) $N_D^T=10^{18}/\mathrm{cm}^3$. Zero bias was maintained across the structure, and the *I layer* was subjected to a uniform generation rate equivalent to 100 mW/cm^2 of band gap radiation. The transient response of the electron and hole density in the center of the device was monitored. Figure 5 shows the electron and hole transients for the switch-on and switch-off transient. As can be seen, after approximately 1 ps the electron density has reached a steady density level at a value approximately three orders of magnitude greater than that without illumination. For times less than 100 ps holes closely follow the electrons, and the densities of both are governed by the generation-recombination times of the continuity equations (1) and (2). The trap rate equations have longer time scales than those of electrons and holes, and prior to 100 ps have not responded to the higher levels of electrons and holes. The response of the deep donors and acceptors is shown in Figure 6. *The electron density relaxes back to its initial value about 1 ps after the illumination is switched off. The electron lifetime appears to be of the order of 1 ps.*

Beyond 100 ps, the ionized donor population begins to decrease slightly in response to the excess electrons. Since the kinetics of the trap rate equations for the specified energy levels and capture coefficients dictate that $N_D^+ \sim N_A^-$, the ionized acceptor concentration also declines.[22] As a result, *the excess optically generated holes can no longer recombine at the same rate as the electron and the hole density begins to rise again.* A new equilibrium is finally reached after about 1 ms, where the hole concentration is approximately 2.5 $\times 10^3/\mathrm{cm}^3$. This value is the difference between the ionized acceptors and donors, i.e., $0=N_D^+-N_A^-+h-e \sim N_D^+-N_A^-+h$, where $e \ll h \ll N_D^+, N_A^-$.

During switch-off, the level of ionized traps does not begin to return to the dark levels until almost a microsecond has elapsed. But the most dramatic feature of this figure is that the transients for the deep donors and acceptors, as shown in Figure 6, are almost identical (to the resolution of the figure they appear exactly the same). This is because of the relatively large levels of the ionized traps, compared to the density of the photogenerated carriers, particularly the holes. From Figure 5 recall that during the long time scale portion of the hole transient the hole density increases from

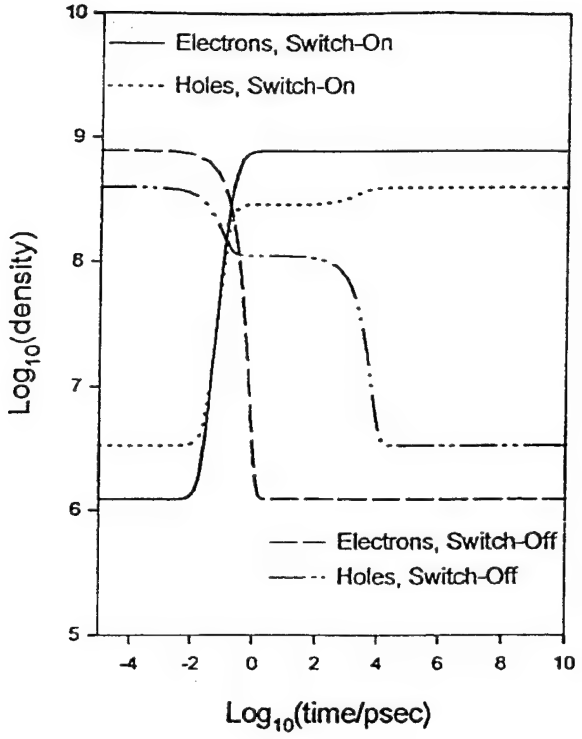

FIG. 7. As in Figure 5 with the following change: the hole capture coefficient was increased to the value of the electron capture coefficient.

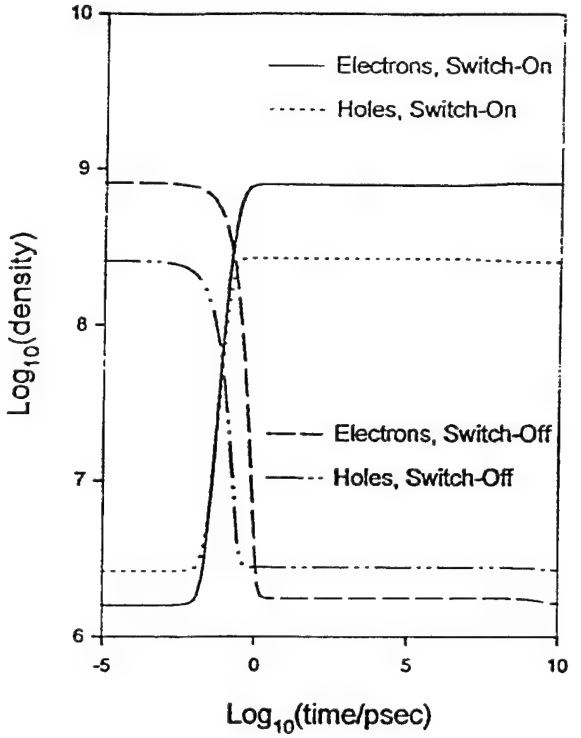

FIG. 8. As in Figure 5, with the following changes: the hole capture coefficient was increased to the value of the electron capture coefficient and the energy levels of the donor and acceptor traps were placed equally from the conduction and valence bands.

$10^9/cm^3$ to $10^{14}/cm^3$, which represents a small perturbation compared to the ionized defect densities, which are of the order of $10^{17}/cm^3$. Thus, the levels of the ionized defects change only slightly from the equilibrium levels and, due to the long time scales over which the changes occur, they remain in near equality with each other. The small overall change in the ionized defect density which does occur is made in an effort to maintain charge neutrality.

The origin of the secondary time scale observed in Figure 5 was traced to the value of the hole capture coefficient, C_p. By increasing this coefficient to a value equal to that of the electron coefficient, C_n, the results shown in Figure 7 were obtained, where we still observe a secondary hole time scale; however, it does not result in a significant increase in the hole density. The decay of the holes, however, is still significantly longer than that of the electrons. Another contribution to the differences between the electron and hole lifetime was found to be due to the relative position of the deep level traps in the energy band. By placing the deep level donors and acceptors equally from the conduction and valence bands, respectively, the results of Figure 8 were obtained. Under these conditions, both electron and hole lifetimes are close to 1 ps, and no secondary time constants are apparent.

How do the above results translate into an understanding of the LT devices of the type discussed by Ibbetson *et al.*?[21] The results, of course suggest that transient measurements are necessary to fingerprint non-stoichiometric materials. To illustrate this, an academic problem was simulated: the transient response of the 2 μm long structure of Figure 4 to optical radiation. The results of this calculation, shown in Figure 9, display the sensitivity of the switch-off transient to the value of the capture coefficients. Individual calculations are for (i) normal capture coefficients, (ii) coefficients an order of magnitude larger, and (iii) coefficients two orders of magnitude larger. For the case of the nominal capture coefficients the band gap radiation is at a level of 100 mW/cm^2. The radiation was adjusted for variations in the capture coefficients to enable the initial densities to be the same. The calculation of Figure 9 demonstrates that transients are sensitive to the capture coefficients, even when the *IV* curves are not. The transients are also sensitive to the density of the traps, even when the *IV* curves are not (see Figure 10). At the very least, these calculations suggest that dc measurements are not sufficient to characterize non-stoichiometric GaAs.

While the above transient calculations demonstrate the sensitivity of device performance to the time constants, the consequences of differences in the electron and hole time constants will be a significant factor in assessing device performance. To illustrate this a simple thought experiment was conducted: For an NIN structure *under bias* we examined the response to a photoexcitation of 10 ps with a repetition rate of 10 ps. Over ten cycles of 10 mW photoradiation, the electrons appear to relax to a value close to their initial value. However, the hole density does not relax to the initial state at the beginning of each cycle, due to the longer relaxation time. As a result, over a large number of cycles, the excess

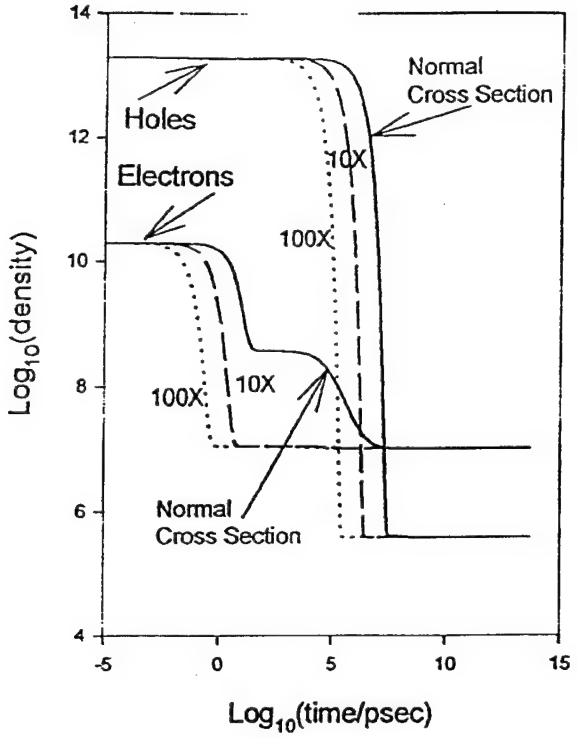

FIG. 9. Transient response of electrons and holes in the center of the 2 μm I region of the NIN structure of Figure 4 following the switch-off of band gap radiation. Capture cross section was varied (10x denotes an order of magnitude increase in cross section, etc.). The radiation intensity was varied such that the initial carrier densities were the same.

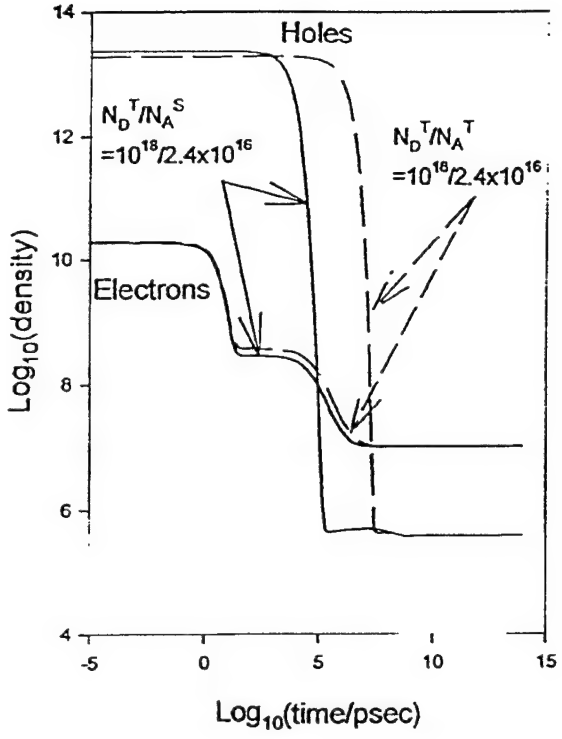

FIG. 10. Transient response of electrons and holes in the center of the 2 μm I region of the NIN structure of Figure 4 following the switch-off of 100 mW/cm^2 band gap radiation. Parameter variation is the acceptor trap density.

holes accumulate and the current transient exhibits drift. When the hole lifetime is the same order as the electrons, both electrons and holes respond equivalently to the light pulse and the current transients are repetitive. These results suggest, at the very least, that the pulse duration and the repetition rate must be adjusted for the slowest carrier.

VII. TWO-DIMENSIONAL CONTRIBUTIONS

While one-dimensional simulations are useful, two-dimensional effects are expected to play an important role in the design of devices. Such a two-dimensional study would carry us beyond the scope of this discussion, but some comments are in order. For example, when considering precipitates, multidimensional transport would result in carrier flow between precipitates which, depending upon the level of injection, would begin to reduce the size of any depletion zone surrounding the precipitate. For the homogeneous distribution of traps considered here, the two-dimensional effects are concerned with the distribution of photogenerated carriers. In the one-dimensional studies, the photogeneration is assumed to be uniform in a direction parallel to the surface. In two dimensions the generation decays with distance from the surface due to absorption of photons. In preliminary studies, with the photon flux and generation terms given as, e.g., $\Gamma=\Gamma_o e^{-\alpha x}$, and $G=\alpha\Gamma$ where Γ_0 is the photon flux transmitted through the surface (Γ_0 is computed from the optical power $\Gamma_o=P_{\text{opt}}/h\nu$, where $\nu=c/\lambda$, α is the optical absorption coefficient, and x is the distance of penetration measured along the optical path, in this case normal to the device surface) the optically generated charge density shows a similar exponential variation. However, at low power levels the charge density was not great enough to affect the potential distribution across the device. Thus, while there is an x direction in optically generated charge, the resulting current is directed only in the direction normal to the contacts. At higher optical power levels, the density of the photogenerated charge would increase and at some point would affect the potential distribution, creating an x direction field. The current paths under such conditions will be more complex than those addressed here.

VIII. INVESTIGATION OF PRECIPITATE MODELS: DEFECT VERSUS BURIED SCHOTTKY

While the previous discussion demonstrates that ignoring the presence of precipitates and assuming a homogeneous distribution of donor and acceptor defects at high concentration can apparently account for such characteristics as resistivity, transients, and shallow donor dependence, *the presence of precipitates must be included.* We consider the two different precipitate models mentioned earlier: *the defect-precipitate model,* and *the Schottky barrier precipitate model.*

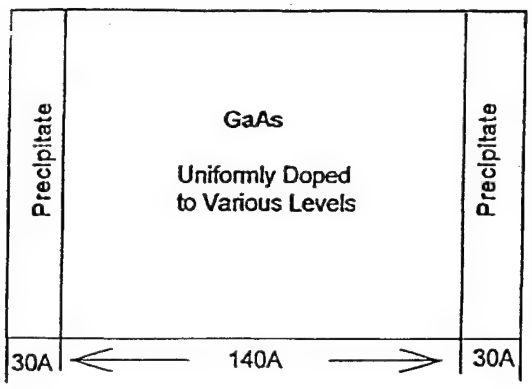

FIG. 11. One-dimensional planar structure for initial precipitate simulations.

IX. DEFECT-PRECIPITATE MODEL (DPM), PLANAR GEOMETRY

The defect-precipitate model assumes that the precipitate sites in annealed LT GaAs contain high local concentrations of defects. Assuming precipitates on the order of 60 A in diameter at a density of $10^{17}/cm^3$, and a total defect density of $10^{18}/cm^3$, the density of defects within a precipitate would be $8.85\times10^{19}/cm^3$ if all the defects were concentrated within the precipitates. We further assume that these precipitates are periodically distributed throughout the material at a spacing of 200 A, which is consistent with a density of 10^{17} precipitates/cm^3.

Initial simulations were performed using a one-dimensional planar geometry to illustrate key qualitative features of the problem. Two precipitates were modeled, as shown in Figure 11. The ratio of donor to acceptor defects in the precipitate regions was set to yield an equilibrium Fermi level 0.8 eV below the conduction band, which from Figure 2 requires approximately the same density for each type of trap. The electron distributions for shallow doping densities between $2\times10^{17}/cm^2$ and $2\times10^{19}/cm^3$ are shown in Figure 12. These results indicate that the inter-precipitate material would remain semi-insulating until the doping level reached $2\times10^{19}/cm^3$, assuming that all shallow donors were ionized. We have not included the effects of degeneracy here. The clusters of defects making up the precipitate are able to trap the majority of charge from the shallow doped region provided the shallow doping level does not exceed a value that depends upon the trap density in the precipitate. At a doping level of $1\times10^{19}/cm^3$ the peak electron density is on the order of only $10^{11}/cm^3$.

Figure 13 shows the level of ionized donors and acceptors in the precipitate regions for a shallow donor level of $2\times10^{19}/cm^3$, at which the structure should be regarded as conductive. To interpret this figure, it should be understood that under undoped conditions the densities of ionized donor and acceptor traps in the precipitates are the same, and equal to, the total acceptor trap density (acceptor trap density is below that of the donor trap density). Thus, the figure shows that the deep donors near the surface of the precipitate are being neutralized by trapping an electron from the shallow donor. Continued increase in the shallow donor level results in further neutralization of the ionized deep donors. *The results displayed in Figures 12 and 13 also depend upon the inter-precipitate separation. Additional calculations indicate that as this separation increases the peak doping density at which the material remains resistive is reduced.* While not shown, the potential energy distribution accompanying the above charge distribution is similar to that at a Schottky barrier. For DPM, the effective barrier height is dependent on the density of the shallow dopants surrounding the cluster, since the trap kinetics within the cluster determine the electron density within the cluster, which in turn depends upon the surrounding doping level.

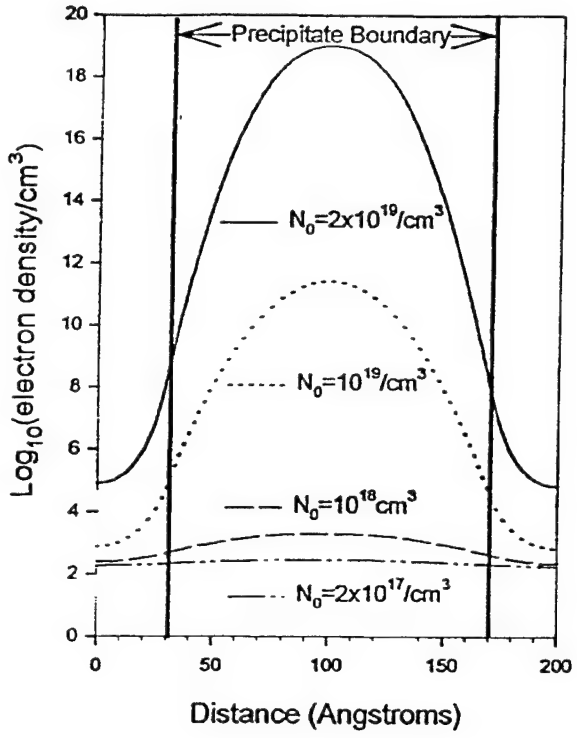

FIG. 12. Electron distribution between and within the vicinity of defect precipitates. For this calculation $E_C-E_F=0.8$ eV, $N_D^T=8.84\times10^{19}/cm^3$, $N_D^T/N_A^T=1.014$, and the concentration of shallow donors was varied.

These above results suggest that precipitates consisting of a high concentration of defects can *also* account for the dc semi-insulating properties of LT GaAs (see Table I). But these planar defect precipitate models can only be viewed as qualitative, since the assumption of a planar geometry is erroneous. Planar geometries allow excess depletion (compared, e.g., to spherical geometries) because the number of free electrons available to be trapped and the number of deep level trapping sites vary linearly with distance from the interface between the precipitate and the inter-precipitate material. Spherical geometries, discussed below, provide a more realistic representation of a single precipitate, since the number of electrons to be depleted would increase with the cube of the distance from the precipitate boundary, and the number of trap sites would decrease with the cube of the radius as we move towards the center of the precipitate.

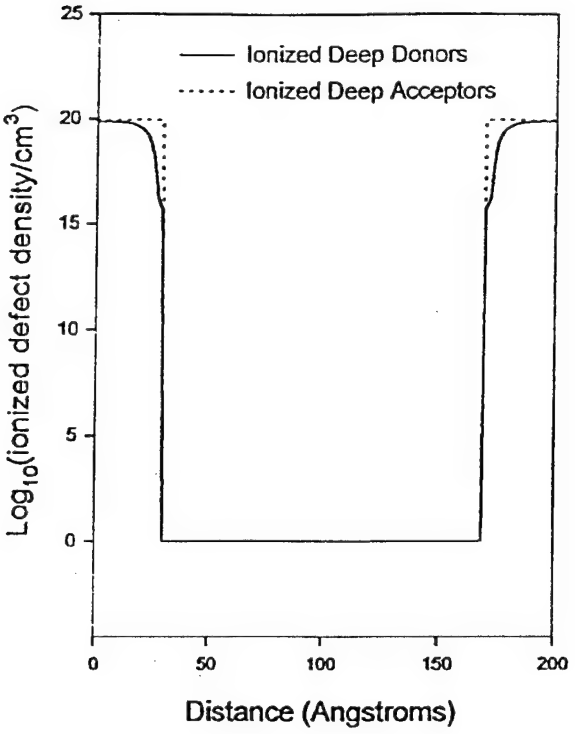

FIG. 13. Distribution of ionized defects for the Figure 12 calculation, and $N_0=2\times10^{19}/cm^3$.

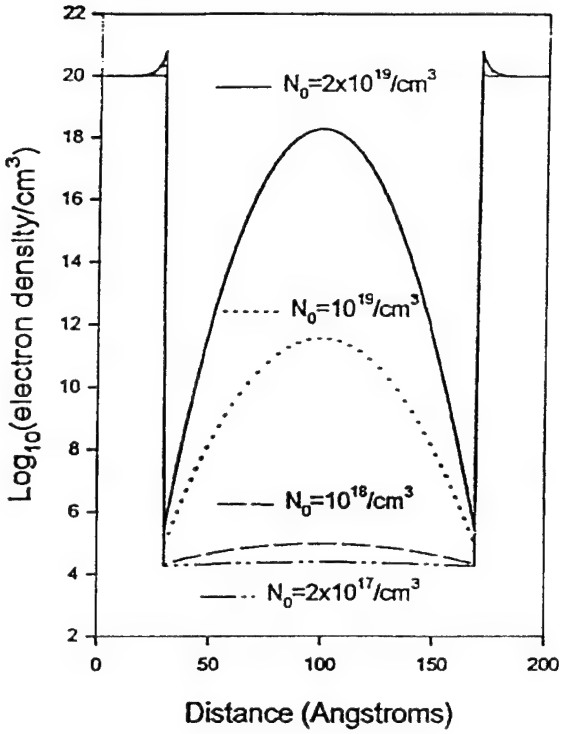

FIG. 14. Electron distribution between and within the vicinity of Schottky barrier precipitates. For this calculation the barrier height was 0.8 eV, and the concentration of shallow donors was varied.

Thus, spherical geometry would not result in such high levels of depletion for the same density of defects in the precipitate.

X. SCHOTTKY BARRIER PRECIPITATE MODEL (SPM)

We repeated the simulations of the planar DPM with the precipitate modeled as a Schottky barrier. The modeling of the Schottky barrier was previously discussed, with several illustrations provided in Appendix A. Figure 14 shows the distribution of free electrons between two Schottky barriers for the same shallow doping levels used in the DPM simulations. The barrier height was taken as 0.8 eV. The results are remarkably similar to those of the DPM. At a shallow doping level of $1\times10^{19}/cm^3$ the peak electron density between the barriers is also about $1\times10^{11}/cm^3$. However, at a doping level of $2\times10^{19}/cm^3$ the Schottky barrier precipitate model (SPM) yields a peak density of just over $1\times10^{18}/cm^3$, whereas the DPM yields a significantly higher peak density, close to $1\times10^{19}/cm^3$. Charge neutrality is maintained in this structure by the accumulation of electrons on the "metal" side of the "metal"-semiconductor interface in the SPM, whereas in the DPM ionized donor defects were neutralized, exposing ionized acceptor defects. (Note: in a true metal, whose density is much higher than that represented here, the amount of charge accumulation on the metal side, while consistent with charge neutrality, would be negligible compared to the nominal metallic density.)

XI. SPHERICAL MODELING OF PRECIPITATES: SCHOTTKY BARRIER VERSUS DEFECT MODELS

In view of the qualitative similarity found in planar geometry simulations of the two precipitate models and because planar geometries are unrealistic, we turned our efforts to modeling of precipitates using spherical coordinates. As was stated before, the DPM is able to deplete the adjacent semiconductor material based on the trap sites. In the planar configuration the charge depleted increases linearly and the trap sites available increase linearly with distance from the interface between the precipitate and the semiconductor material. In spherical geometry, the charge depleted decreases with the cube of the depletion region width and the trap sites decrease in a similar manner. Using SPM, the charge depleted is proportional to the surface area of the Schottky barrier and we expect to see a greater deviation between the two models. However, while it was possible to investigate two adjacent precipitates in a planar configuration and verify that depletion regions would overlap, the spherical geometry used here (we are not performing three-dimensional simulations) allows us to *model only a single precipitate,* then, based on planar studies, extrapolate the results to spherically confined precipitates.

XII. SPHERICAL PRECIPITATE-DEFECT SIMULATION

To show the geometric effects we first computed the charge and potential energy distributions for a single precipitate 60 Å in diameter, with $N_D^T/N_A^T=2$ and the donor trap

density in the precipitate set at $8.84\times10^{19}/cm^3$. This yielded a Fermi level near midgap ($E_c-E_f=0.69$ eV) under equilibrium conditions. The material surrounding the precipitate was doped with shallow donors at a level of $1\times10^{18}/cm^3$. Comparisons of the spherical computations and planar approximations are shown in Figures 15a and 15b on linear and log scales. For the spherical geometry the DPM is unable to deplete the surrounding material. Within 15 A of the precipitate surface (a radius of 45 A from the center) the density of electrons in the surrounding material is nominally $1\times10^{17}/cm^3$. At a radius of 100 A the electron density is $6.75\times10^{17}/cm^3$. This suggests that if precipitates were spaced 200 Å apart, the minimum electron density resulting from the overlapping of depletion regions would be on the order of $3\times10^{17}/cm^3$ or greater for a shallow doping level of $1\times10^{18}/cm^3$. This is drastically different from the planar case, where significant depletion is shown to extend well beyond 100 A. Calculations were also performed for a shallow donor density of $1\times10^{17}/cm^3$. While the depletion region extends further than for the $1\times10^{18}/cm^3$ case, at 100 A the density is still on the order of $3\times10^{16}/cm^3$, which would render the material conductive. When the trap ratio is increased to $N_D^T/N_A^T=1.014$, with the same donor concentration of $8.84\times10^{19}/cm^3$, the Fermi energy increases to 0.8 eV and the depletion region broadens, as seen in Figure 15b.[23] *However, even at this deeper Fermi level, the electron density at 100 Å radius is over* $4.3\times10^{17}/cm^3$ *when the surrounding material is doped to* $1\times10^{18}/cm^3$. This would be very close to being on the verge of the boundary between conducting and semi-insulating material when the interaction of several precipitates is considered. From this we can conclude that if precipitates of defects are responsible for the semi-insulating properties of LT GaAs:As, then the semi-insulating properties would be critically dependent on the concentration of defects within the precipitate.

XIII. SPHERICAL SCHOTTKY BARRIER SIMULATIONS

Simulations for the SPM in spherical coordinates show qualitatively similar density profiles to the DPM, as shown in Figure 16. However, there are important differences between the two models. In the DPM, the effective barrier height is set by the position of the equilibrium Fermi level, which varies as the traps in the precipitate are filled. In the SPM, the barrier height remains fixed regardless of the doping condition. The SPM is thus far more linear and, as a result, we expect greater depletion than with the DPM. From Figure 16 we observe that at a shallow doping density of $10^{18}/cm^3$ the free electron concentration at a radius of 100 A is about $3.4\times10^{16}/cm^3$, whereas for the defect model with the equilibrium Fermi level at 0.8 eV, the electron density was $4.3\times10^{17}/cm^3$ at the same doping level. This is over an order of magnitude greater. It is thus apparent that the SPM would yield a more resistive material than the DPM, *unless significantly higher trap levels were present in the DPM precipitate.*

The DPM simulations show that the depletion region is very sensitive to the Fermi level in the precipitate. SPM simulations show an almost negligible change when the bar-

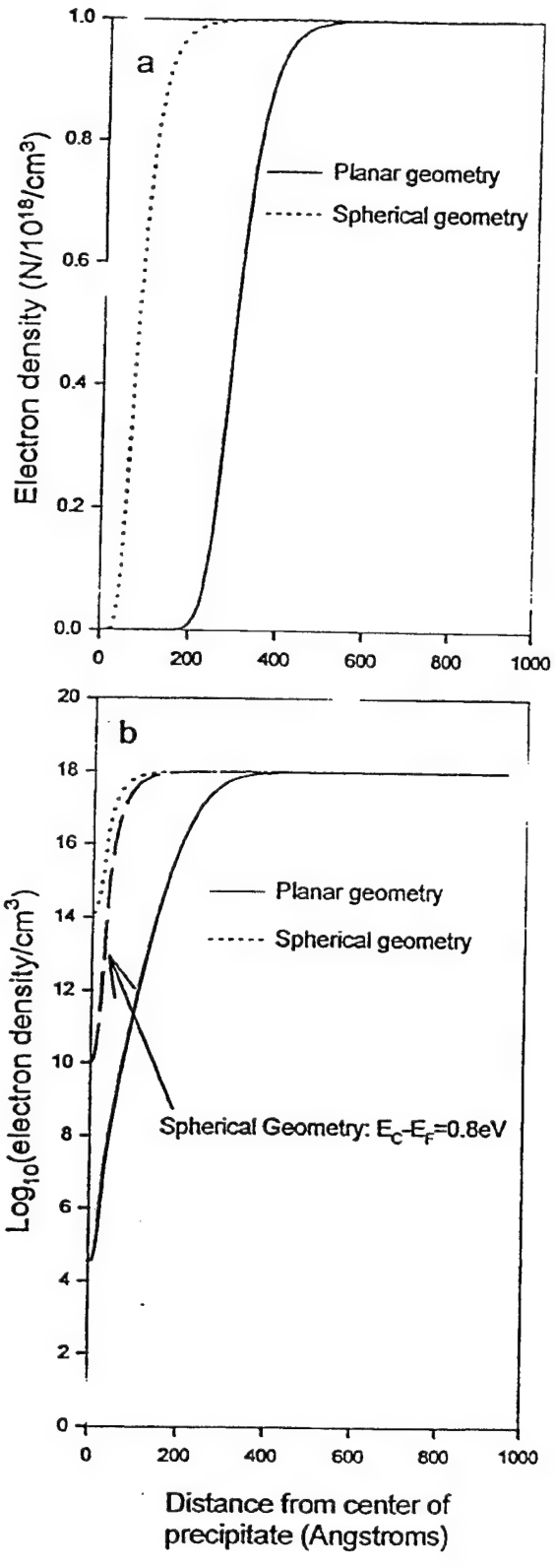

FIG. 15. Comparison of spherical and planar precipitate depletion regions using the DPM with a shallow donor concentration of $N_0=10^{18}/cm^3$ and a deep trap concentration of $N_D^T=8.84\times10^{19}/cm^3$. (a) Linear scale, (b) logarithmic scale. For the solid and dotted lines $E_C-E_F=0.69$ eV, $N_D^T/N_A^T=2$, for the dashed lines $E_C-E_F=0.8$ eV, $N_D^T/N_A^T=1.014$.

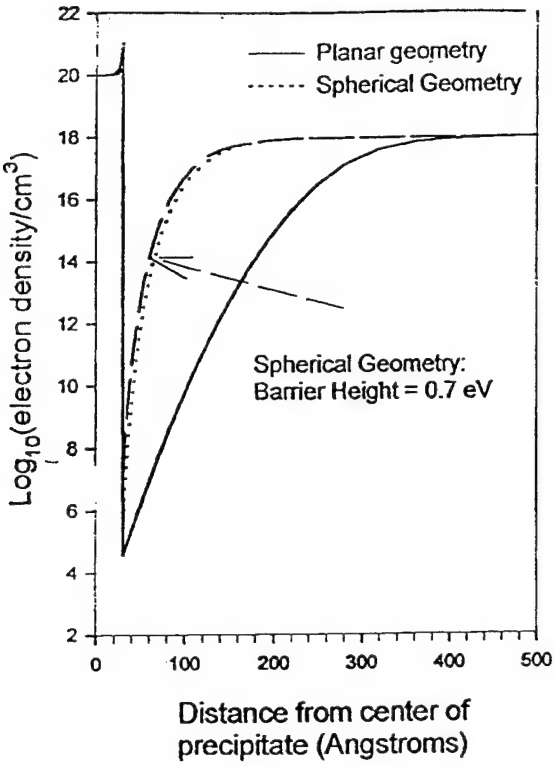

FIG. 16. Comparison of electron density distribution for spherical and planar depletion regions using SPM. For the solid and dotted lines the barrier height is 0.8 eV. For the dashed line the barrier height is 0.7 eV.

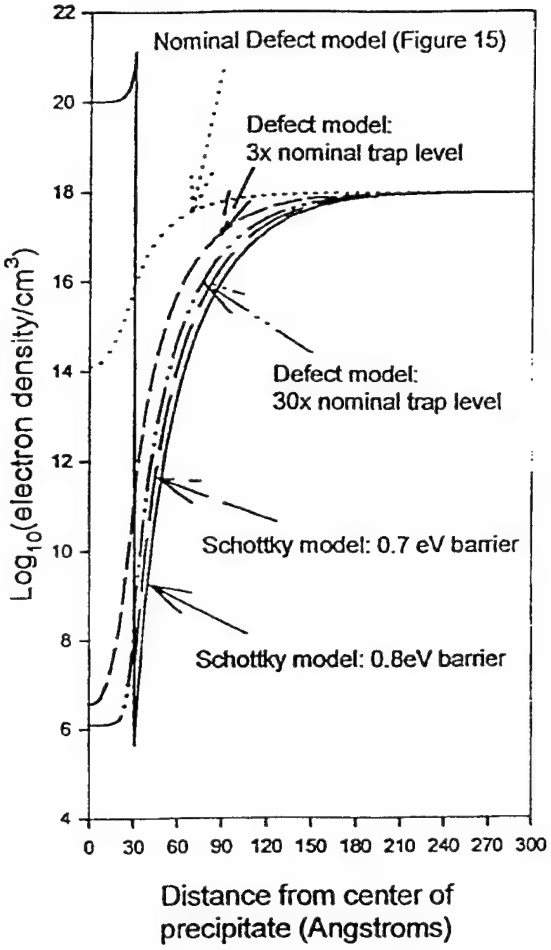

FIG. 17. Electron density distribution for DPM and SPM, with different barrier heights and different trap densities.

rier height is changed, (see Figure 16, dashed line). In Figure 16, the density of electrons at 100 A is $3.8\times10^{16}/cm^3$ for an 0.8 eV barrier and $5.4\times10^{16}/cm^3$ for the 0.7 eV barrier. The difference between the DPM and SPM results is as follows: when undoped, the position of the Fermi level is approximately the same in both models. However, in the DPM when the material is doped, the migration of electrons into the precipitate and neutralization of ionized donor sites results in a movement of the Fermi level towards the conduction band, reducing the depletion width. This feature is absent in the SPM.

The level of traps required in the DPM to yield results similar to the SPM is shown in Figure 17, where it is apparent that even with trap densities 3 times greater than would seem reasonable, the DPM still falls short of the Schottky barrier result at barrier heights of 0.7 and 0.8 eV.

XIV. PHOTO-OPTICAL RESPONSE OF SPM

With reference to Table I, three models have been examined. It was demonstrated that:

(1) a model in which a homogeneous distribution of traps is introduced can account for both the resistive and optical properties of LT GaAs;

(2) a planar geometry model of both the DPM and SPM can also account for the semi-insulating properties of LT GaAs;

(3) in a model with spherical geometry precipitates the DPM framework is very sensitive to the density of traps, and is at the limit of explaining the semi-insulating properties of LT GaAs;

(4) a spherical SPM model can easily account for the dc semi-insulating characteristics of the material.

Based upon these features, a study of the optical response of LT GaAs within the SPM framework was undertaken (similar calculations with the DPM framework produce the same results). This investigation was undertaken using a single precipitate. Optical generation was introduced and the *switch-on* transient state was obtained; the optical generation was then turned off and the transient monitored. The electron density 100 A from the precipitate center was observed as a function of time. *For the case where the material surrounding the precipitate was trap free, it was immediately apparent that the optically generated carriers could only be collected by ambipolar diffusion through the boundary of the computational domain, and that the time scales would be considerably longer than those seen experimentally. Band-to-band time scales also fall into the long time scale category.* In view of the long time constants, we felt that the

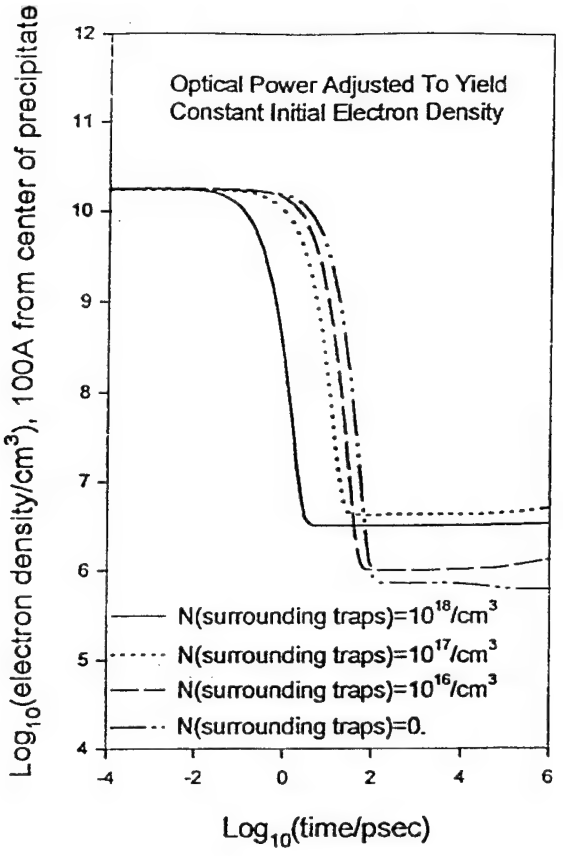

FIG. 18. Transient response of electron density at a point 100 A from the center of a Schottky barrier precipitate, as a function of residual trap density surrounding the precipitate. Optical power was adjusted to yield constant initial electron density.

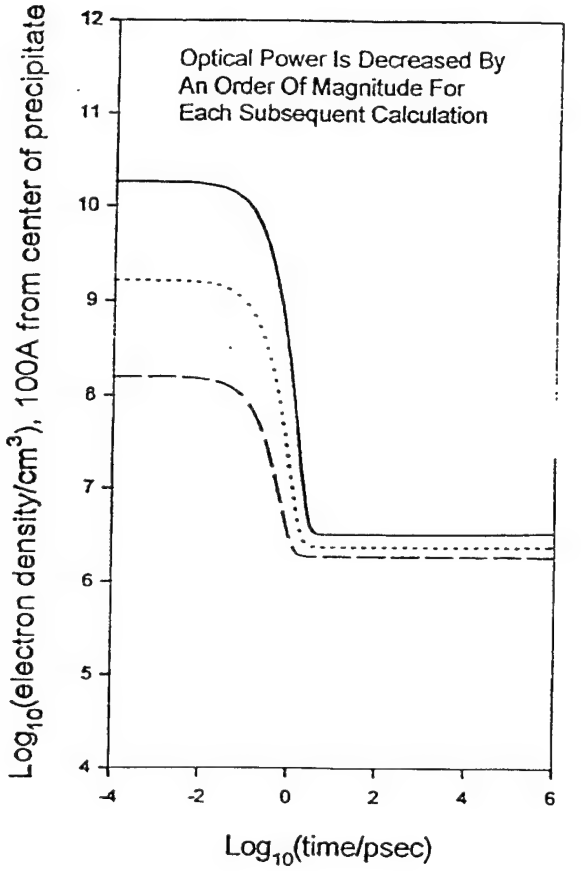

FIG. 19. Transient recovery of a Schottky barrier precipitate from optical radiation as a function of optical power intensity. Residual trap density surrounding the precipitate is $10^{18}/cm^3$. The solid line curve for this figure represents the same data as the solid line curve for Figure 18.

simple SPM was likely to be inadequate, and that enhancements to the SPM and DPM were necessary, in the form of residual traps in the material surrounding the precipitate.

XV. PHOTO-OPTICAL RESPONSE AND CARRIER LIFETIME FOR ENHANCED DPM AND SPM

A series of simulations were performed for the SPM with residual traps in the surrounding material. In the surrounding material $N_D^T/N_A^T=2$ and the residual donor trap density varied from (no residual traps) to $1\times10^{18}/cm^3$. *The surrounding material was void of shallow donors.* (For companion DPM simulations, the defect level in the precipitates was also $N_D^T/N_A^T=2$, with the donor traps set at $8.84\times10^{19}/cm^3$.) The optical illumination was adjusted in intensity so that all relaxation transients started with the same optically generated electron density. Figure 18 shows the transient response of the SPM structures (similar results apply to the DPM) as represented by the electron density time history at a distance of 100 A from the center of the precipitate. The results indicate that picosecond lifetimes are obtained for the case where the defect density in the surrounding material is at the $1\times10^{18}/cm^3$ level. A drop in the defect level to $1\times10^{17}/cm^3$ increases the lifetime to tens of picoseconds. Further reduction in the residual defect density has little effect as the optically generated carriers diffuse through the computational boundary of the simulation in approximately 100 ps. The recovery time for the $10^{18}/cm^3$ calculation is very similar to that of Figure 7; indeed the dependence on trap density follows standard arguments.

Additional *enhanced* calculations were performed with residual traps distributed as *Saturn-type* rings around the precipitate. Enhanced recovery of the transient occurred only in those regions where the trap concentration increased. Calculations were also performed with different values for the capture coefficients. In regions of the shortest recombination times the carriers approached equilibrium on the shortest time scale. *For both the SPM and DPM, the time scales were dominated by the material properties surrounding the precipitate, and not the precipitate.* Some experiments[24] seem to suggest that the defects between the precipitates are negligible. We have no explanation for this discrepancy.

For the modest optical power used in this study, the lifetime of the transient photoresponse is approximately independent of optical power. Figure 19 shows this result for a residual defect density of $1\times10^{18}/cm^3$ over a range of optical power.

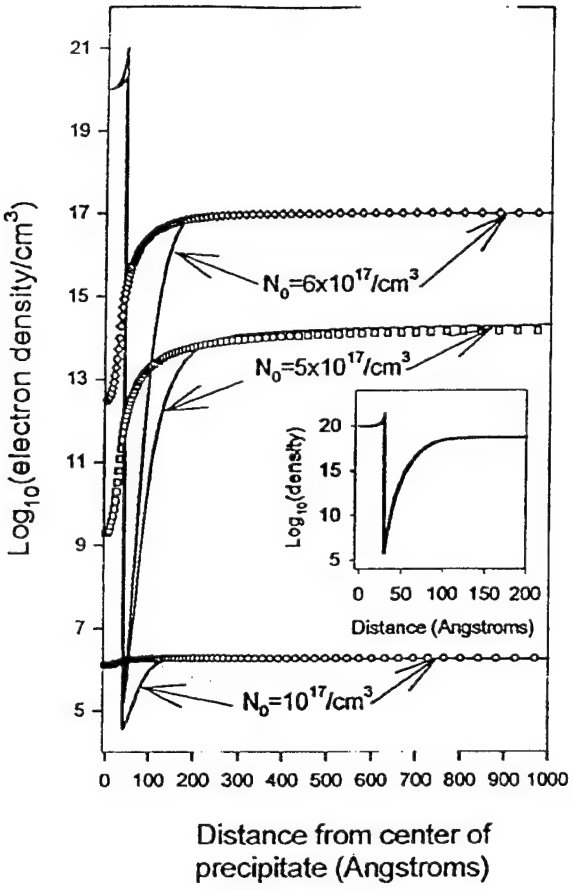

FIG. 20. Comparison of DPM and SPM. Variable is the shallow donor concentration. Solid lines in the figure are all for the Schottky model; symbols are for the defect model. Inset is for SPM with a donor concentration of $6\times10^{18}/cm^3$.

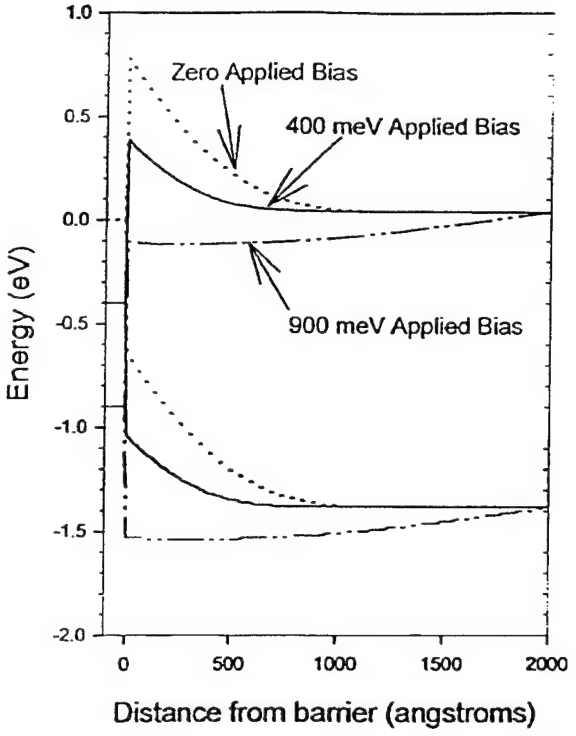

FIG. 21. Conduction and valence band profiles under various bias conditions, using the zero-band gap semi-metal model for the Schottky barrier.

XVI. DEPLETION ZONES, SPHERICAL PRECIPITATES, SHALLOW DONORS

The results of the study suggest that LT GaAs comprised of precipitates with defects in the surrounding material could account for much of the dc and transient behavior of the structure. Within this framework it is necessary to revisit the role of precipitate spacing on the resistivity of the structure. Calculations were performed for both the DPM and SPM with a single spherical precipitate surrounded by defects at a level of $1\times10^{18}/cm^3$ with $N_D^T/N_A^T=2$. Two results were anticipated: first, the material remains semi-insulating for higher concentrations of shallow donors, when compared to the materials without surrounding traps; second, the depletion zones for the Schottky barrier precipitates are broader than those for the defect precipitates.

The results of the simulations are shown in Figure 20, and should be compared to the results of Figures 15 and 16, which were performed for spherical precipitates without any residual traps. The lines in Figure 20 are the SPM results; the symbols are for the DPM. As can be seen, for distances far from the precipitate, the residual defects control the level of free electrons. For the DPM structure at $N_0=5\times10^{17}/cm^3$ the free electron concentration is only about $1\times10^{14}/cm^3$; as the doping level is raised slightly, the electron concentration rises rapidly. By contrast, for the SPM structure at a donor density of $6\times10^{17}/cm^3$, the free-carrier density at 100 A from the center of the precipitate is approximately $2\times10^{14}/cm^3$. Thus, if we were dealing with precipitates that were separated by a distance of 200 A only the SPM would yield semi-insulating material. For this structure the transition to conducting material occurs with a donor density of approximately $6\times10^{18}/cm^3$. The inset to Figure 20 shows the density distribution for this higher donor level, where at 100 A from the center of the precipitate the density is near its maximum attainable value.

XVII. CONCLUSIONS

We have performed a series of simulations aimed at modeling the physical properties of *annealed* LT GaAs and gaining an understanding of the role and character of the precipitates which appear in the material. The results of the study, as summarized in Table I, indicate that *isolated* calculations that ignore such fundamental details of the material characteristics as precipitates can explain the dc and phototransients. *Since the experimental observation of precipitates means they are not to be ignored*, when precipitates are included in the study it was concluded that all of the experimental results including transients can be explained, provided the precipitates are surrounded by residual defects. The uniformity of the residual defect distribution is less of an issue than is the concentration of residual defects and the

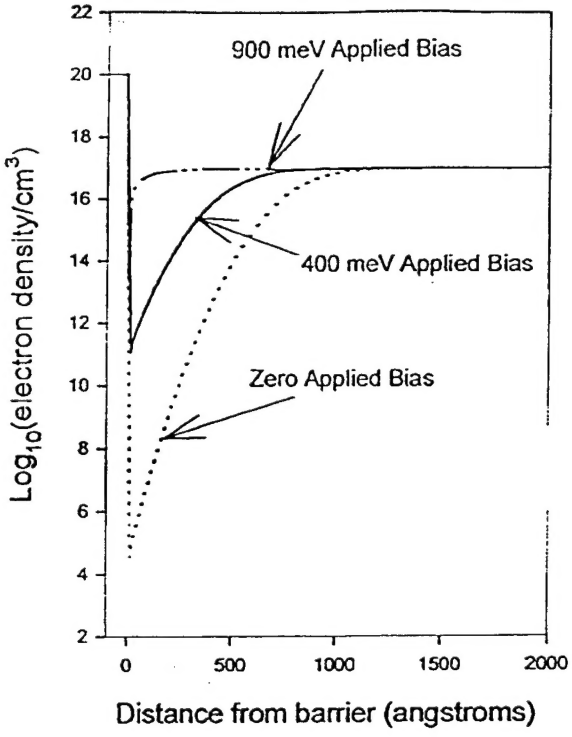

FIG. 22. Electron density profiles under various bias conditions, corresponding to Figure 21.

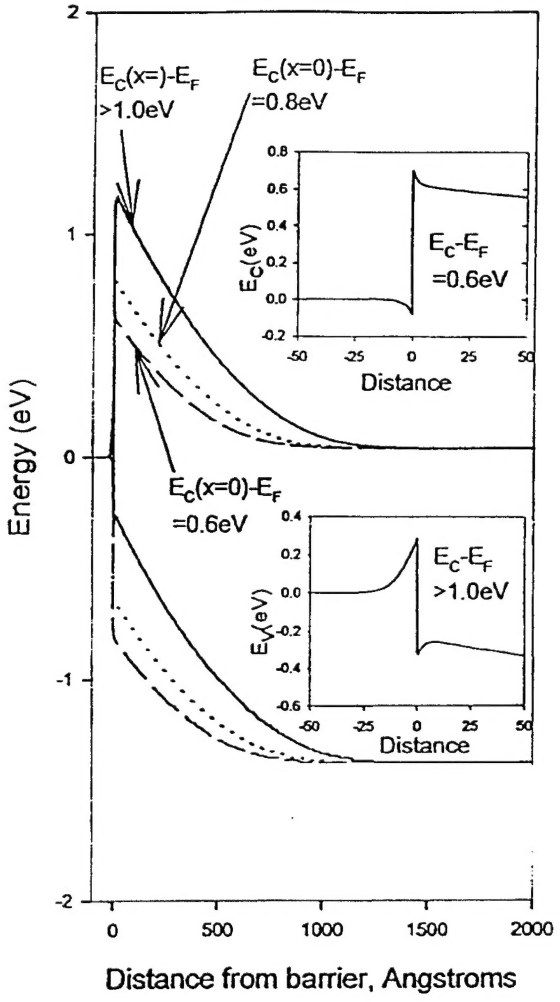

FIG. 23. For the structure of Figure 21, with a nominal Schottky barrier height of 0.8 eV, the variation of the conduction and valence band as the defect density surrounding the barrier is changed. Insets denote blowups in the vicinity of the interface of, respectively, the conduction band (for a Fermi level of 0.6 eV below the conduction band) and the valence band (for a Fermi level greater that 1.0 eV below the conduction band).

values of their associated capture coefficients. While it is not possible to say definitively whether the precipitates in LT GaAs act as buried Schottky barriers, or whether the precipitates are clusters of defects, the experimental evidence strongly suggests that the precipitates are not electrically passive, and the simulations suggest that they are more likely to be buried Schottky barriers. The requirement of traps between precipitates is not consistent with the conjecture of Luo *et al.*,[18,19] as hopping conduction in annealed material with intra-precipitate traps would render the material conductive. Additional study in this area is clearly called for.

By way of demonstration, the simulation results clearly indicate that dc measurements will not adequately provide a clear picture of the material properties of LT GaAs —transient measurements are also required. The issue of multidimensional effects is briefly mentioned in the study. It is worthwhile emphasizing that after multidimensional calculations are performed some of the conclusions of this article may be altered, particularly with respect to such features as the device length dependence of the dc *IV* measurements. For here we expect that as carriers are injected into the nonstoichiometric material, they will begin to alter the size of the depletion zones surrounding the precipitate, and thereby alter the voltage at which the current reaches the trap-filled limit. It is not likely that the arguments concerning the transients will be altered by moving to three dimensions.

ACKNOWLEDGMENTS

Effort sponsored by the Air Force Office of Scientific Research, Air Force Material Command, USAF under Grant No. F4962 -94-C-0024. The U.S. Government is authorized to reproduce and distribute reprints for governmental purposes notwithstanding any copyright notation thereon. The authors are grateful for this support. The authors benefited from numerous discussions with G. Witt, J. Woodall, M. Melloch and P. Fauchet.

APPENDIX A: THE SCHOTTKY BARRIER MODEL

Prior to implementing the LT GaAs Schottky barrier precipitate simulation model, we performed a number of planar geometry simulations of a Schottky barrier on *n* and *p* type material to verify that the model gave qualitatively meaningful results. The buried Schottky barriers were represented as: (1) a zero band gap semiconductor with a specified offset voltage with respect to GaAs, in which (2) the electron and hole density are equal and high and where (3) everywhere within the material, except at the region surrounding the

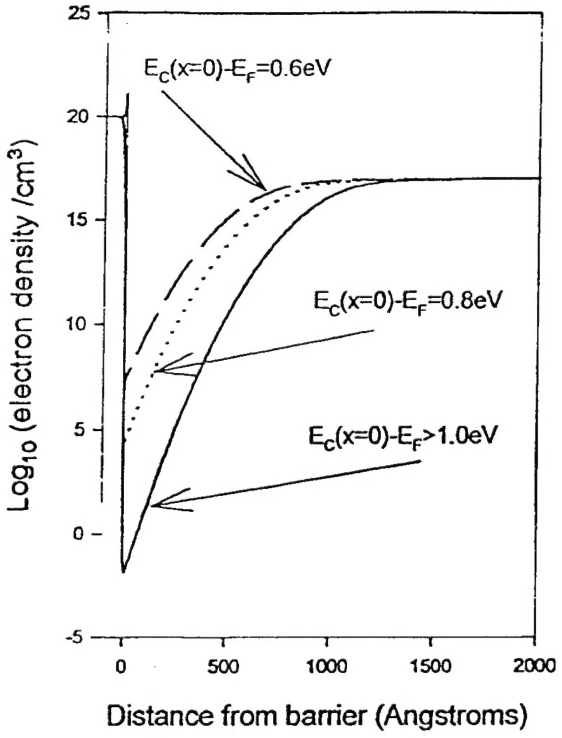

FIG. 24. Electron density distribution as determined by the potential distribution of Figure 23 and Poisson's equation.

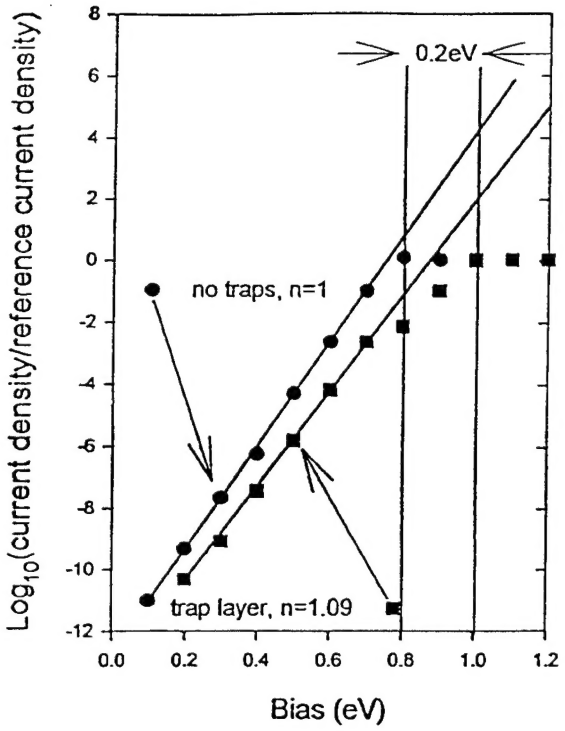

FIG. 25. Current–voltage characteristics for a simple Schottky barrier precipitate, and one surrounded by defects where $E_C(x=0)-E_F>1.0$ eV. The reference current density is 1.6×10^5 A/cm^2.

boundary of the zero band gap material and the GaAs material, there was local charge neutrality. We have not tried to fine tune the model to duplicate experimental results. (Note: the boundaries of the computational domain are treated as ohmic contacts, following standard drift and diffusion practices.) This appendix summarizes the study.

The first simulations were for a 0.8 eV barrier (conduction band) on n type material doped to 1×10^{17}/cm^3. Figure 21 shows the band structure for this configuration at bias levels of 0.0, 0.4, and 0.9 eV. The maximum depletion occurs under zero applied bias, represented by the dotted lines. The corresponding electron density is shown in Figure 22. These results are similar to those found in any textbook.[25]

Introducing a layer of traps in the vicinity of the Schottky barrier alters the effective barrier height. To demonstrate this a donor defect sheet density fixed at 1×10^{13}/cm^2 was placed across a 100 Å layer and the acceptor defect level was varied to change the Fermi level. Results are presented for zero bias in Figure 23 and identified by the position of the Fermi level. With a trap ratio such that the Fermi level was at 0.8 eV (Figure 23, dotted line), the band structure is effectively unaltered from the case of a Schottky barrier alone. When the trap ratio yields a Fermi level of 0.6 eV (Figure 23, dashed line) or somewhat greater than 1.0 eV (Figure 23, solid line) a local redistribution of charge occurs at the interface. For a Fermi level of 0.6 eV there is a narrow spike in the conduction band (topmost inset to Figure 23, where we show conduction band energy over a 100 A region centered about the interface). For a Fermi level >1.0 eV, there is a narrow spike in the valence band (bottom inset to Figure 23). The corresponding electron density plots are shown in Figure 24. The spike in electron density is a Fermi level of 0.6 eV, and occurs within the 'metal'. For a higher density 'metal' this change in concentration would be negligible. For a Fermi level >1.0 eV, there is a decrease in density on the 'metal' side.

These results indicate the sensitivity of the Schottky barrier contact to the material properties of the surrounding region. This is demonstrated further in Figure 25 where we display the forward current–voltage characteristics for the ordinary Schottky barrier (closed circles) and for a barrier with a trap layer which increases the effective barrier height by 0.2 eV (closed squares). The solid lines are obtained from the equation

$$\log_{10}(J/\text{Reference Current}) = \log_{10}\left[\exp\frac{[V-n_{\text{effective barrier height}}]}{nk_BT}\right],$$

where n in the above equation is the ideality factor.[26] For the calculation without traps, $n=1$, and the extrapolated effective barrier height is 0.76 eV, which is somewhat less than the input of 0.8 eV. For the calculation with traps $n=1.09$. and the extrapolated effective barrier height is approximately 0.8 eV. Notice that both curves show current saturation, with the trap layer structure leading into saturation at a value of bias approximately 0.2 eV higher than that of the study without traps. The current voltage characteristics for the latter also exhibit additional structure at the higher bias levels, that

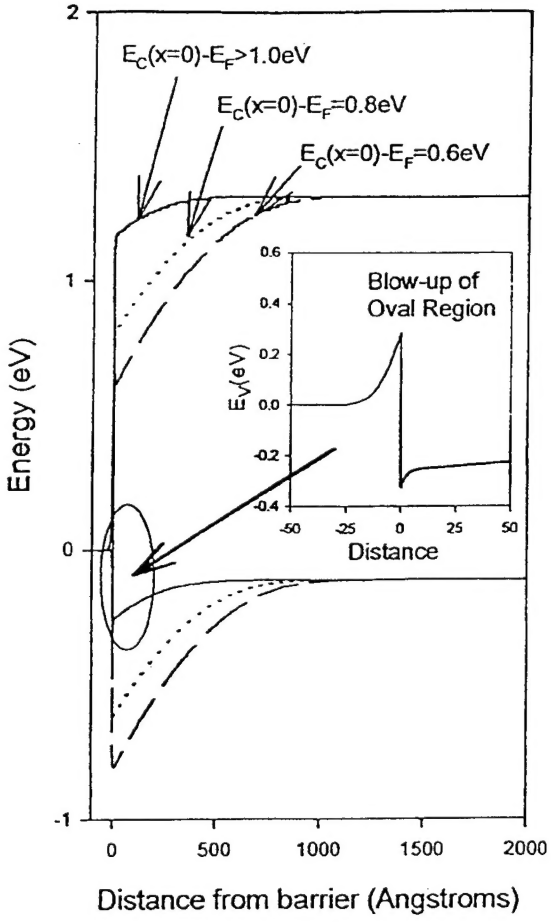

FIG. 26. As in Figure 23, but for p-type material. Inset is a blowup of the valence band for the case when $E_C(x=0)-E_F>1.0$ eV.

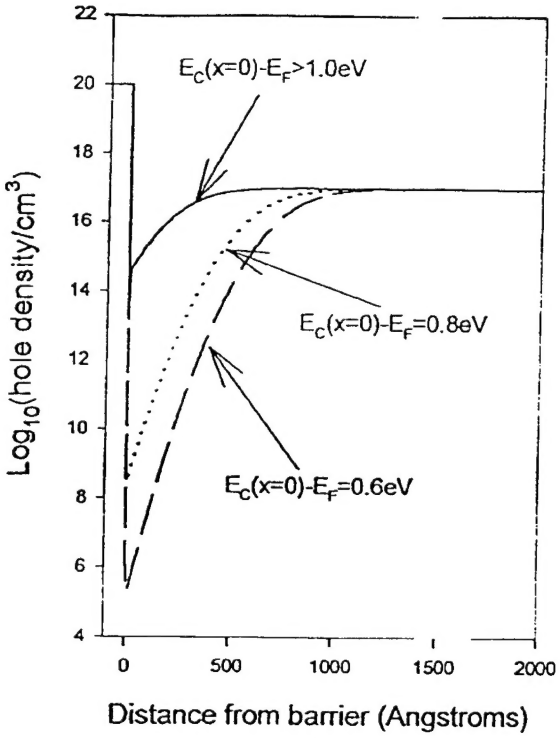

FIG. 27. The hole density corresponding to the potential distribution of Figure 26.

arises from the filling of traps in the vicinity of the 'metal'-semiconductor interface. Apart from this difference, both curves show classical exponential behavior prior to saturation.

Finally, Figures 26 and 27 show results for the same structures presented in Figures 23 and 24, but with the semiconductor material doped to $1\times10^{17}/\text{cm}^3$ p type. The results are as expected, and serve to demonstrate the applicability of the model to both n and p type materials.

APPENDIX B: CAPTURE COEFFICIENTS, THE MOBILITY MODEL AND PRECIPITATE DENSITY

The baseline capture coefficients used in this study were:

$$C_n=10^{-5}\text{cm}^3/\text{s}\quad C_n^+=1.31\times10^{-5}\text{cm}^3/\text{s}$$

$$C_p=2.6\times10^{-10}\text{cm}^3/\text{s}\quad C_p^-=10^{-5}\text{cm}^3/\text{s}. \tag{B1}$$

The following field dependent mobility model is used in this study. For undoped material:

$$\mu_n=\mu_{n0}\frac{1+\left(\frac{v_{ns}}{\mu_{n0}E}\right)\left(\frac{E}{E_0}\right)^4}{1+\left(\frac{E}{E_0}\right)^4}\qquad \mu_p=\mu_{p0}\frac{1}{1+\frac{\mu_{p0}E}{v_{ps}}}, \tag{B2}$$

where:

$$\begin{aligned}&\mu_{n0}=8000\ \text{cm}^2/\text{Vs}\\ &\mu_{p0}=400\ \text{cm}^2/\text{Vs}\\ &v_{ns}=8.5\times10^6\ \text{cm/s}\\ &v_{ps}=1.0\times10^7\text{cm/s}\\ &E_0=4000\ \text{V/cm}.\end{aligned} \tag{B3}$$

For the case of doping in n-type material, the constant mobility in the above expressions is replaced by:

$$\mu_0=\frac{8000\ \text{cm}^2/\text{V s}}{\sqrt{1+\frac{\text{Net Ionized Sites Density}}{10^{17}/\text{cm}^3}}}, \tag{B4}$$

where the net ionized density includes the shallow donor and acceptors and the deep donors and acceptors. Equation (B4) is a result of fitting empirically obtained data.

In calculating the precipitate density in the spherical DPM discussion, we assumed the following: precipitate diameter: $P_{\text{diam}}=60$ A; precipitate density: $P_{\text{density}}=10^{17}/\text{cm}^3$; defect density: $D_{\text{density}}=10^{18}/\text{cm}^3$; Number of

defects/precipitate: $D_{density}/P_{density}=10$. In a sphere of diameter 60 Å, the density of defects per precipitate is: $[D_{density}/P_{density}]/(4/3)\pi R^3 = 8.84\times10^{19}/cm^3$.

[1] F. W. Smith, A. R. Calawa, C. L. Chen, M. J. Manfra, and L. J. Mahoney, IEEE Electron Device Lett. 9, 77 (1988).

[2] C. L. Chen, F. W. Smith, A. R. Calawa, L. J. Mahoney, and M. J. Manfra, IEEE Trans. Electron Devices 36, 1546 (1989).

[3] M. Y. Frankel, J. F. Whitaker, G. A. Mourou, F. W. Smith, and A. R. Calawa, IEEE Trans. Electron Devices 37, 2493 (1990).

[4] A. C. Warren, J. H. Burroughs, J. M. Woodall, D. T. McInturff, R. T. Hodgson, and M. R. Melloch, IEEE Electron Device Lett. 12, 527 (1991).

[5] D. C. Look, D. C. Walters, M. O. Manasreh, J. R. Sizelove, C. E. Stuz, and K. R. Evans, Phys. Rev. B 42, 3578 (1990).

[6] M. O. Manasreh, D. C. Look, K. R. Evans, and C. E. Stutz, Phys. Rev. B 41, 102 (1990).

[7] H. Yamamoto, Z.-Q. Fang, and D. C. Look, Appl. Phys. Lett. 57, 1537 (1990).

[8] K. P. Korona, M. Kaminska, J. M. Baranowski, and E. R. Weber, Mater. Sci. Eng. B 22, 41 (1993).

[9] M. Kaminska, E. R. Weber, Z. Liliental-Weber, R. Leon, and Z. U. Rek, J. Vac. Sci. Technol. B 7, 710 (1989).

[10] P. Haulojärvi, J. Mäkinen, S. Palko, K. Saarinen, C. Cabel, and L. Lisykay, Mater. Sci. Eng. B 22, 16 (1993).

[11] Z.-Q. Fang, and D. C. Look, Appl. Phys. Lett. 63, 219 (1993).

[12] S. A. McQuaid, R. C. Newman, M. Missous, and S. O'Hagan, Appl. Phys. Lett. 61, 3008 (1992).

[13] A. C. Warren, J. M. Woodall, J. L. Freeouf, D. Grischkowsky, D. T. McInturff, M. R. Melloch, and N. Otsuka, Appl. Phys. Lett. 57, 1331 (1990).

[14] R. M. Feenstra, A. Vaterlaus, J. M. Woodall, and G. D. Pettit, Appl. Phys. Lett. 63, 2528 (1993).

[15] A. C. Warren, N. Katzenellenbogen, D. Grischkowsky, J. M. Woodall, M. R. Melloch, and N. Otsuka, Appl. Phys. Lett. 58, 1512 (1991).

[16] D. C. Look, Thin Solid Films 231, 61 (1993).

[17] J. F. Whitaker, Mater. Sci. Eng. B 22, 61 (1993).

[18] J. K. Luo, H. Thomas, D. V. Morgan, and D. Westwood, Appl. Phys. Lett. 64, 3614 (1994).

[19] J. K. Luo, H. Thomas, D. V. Morgan, and D. Westwood, J. Appl. Phys. 79, 3622 (1996).

[20] K. Horio, T. Ikoma, and H. Yanai, IEEE Trans. Electron Devices 33, 1242 (1986).

[21] J. Ibbetson and U. Mishra, Appl. Phys. Lett. 68, 3781 (1996).

[22] Examining the recombination terms in the continuity equations arising from the traps, we have $R_n = C_n N N_A^0 + C_n^+ N N_D^+$, and $R_p = C_p^- P N_A^- + C_p P N_D^0$. At equilibrium, with $N_D^T = 10^{18}/cm^3$, $N_A^T = 5\times10^{17}/cm^3$, $N_D^+ = N_D^0 = 5\times10^{17}/cm^3$, $N_A^- = 5\times10^{17}/cm^3$, and $N_A^0 = 0$. Thus, initial electron and hole recombination takes place on time scales, respectively, $\tau_n \approx 1/C_n^+ N_D^+ = 0.15$ ps, and $\tau_p \sim 1/N_A^- C_p^- = 0.2$ ps. On longer time scales the term involving N_A^0 is small because $N_A^0 \ll N_D^+$. However, in the hole equation, $N_A^- \sim N_D^0$ and a second time constant $\tilde{\tau}_p = 1/C_p N_D^0 = 7.7$ ns is present. This same term appears in the trap rate equation and is responsible for upsetting the balance between ionized deep donors and acceptors on the long time scale which results in the long time increase in hole density.

[23] While the use of the approximate equations (12) and (13) is not likely to be correct for the situation when the Fermi energy is approximately equal to the energy of the donor trap, this figure does display the qualitatively correct result showing the extreme sensitivity to the position of the Fermi level.

[24] M. Melloch (private communication).

[25] S. M. Sze, *Semiconductor Devices, Physics and Technology* (Wiley, New York, 1985).

[26] A. G. Milnes and D. L. Feucht, *Heterojunctions and Metal-Semiconductor Junctions* (Academic, New York, 1972) Sec. 7.4.